International Journal of Bifurcation and Chaos, Vol. 10, No. 5 (2000) 997–1018

CHAOS IN THE REORIENTATION PROCESS OF A DUAL-SPIN SPACECRAFT WITH TIME-DEPENDENT MOMENTS OF INERTIA

M. IÑARREA*
Departamento de Química,
Area de Física Aplicada,
Universidad de la Rioja, 26004 Logroño, Spain

V. LANCHARES†
Departamento de Matemáticas y Computación,
Universidad de la Rioja, 26004 Logroño, Spain

Received April 16, 1999; Revised September 20, 1999

We study the spin-up dynamics of a dual-spin spacecraft containing one axisymmetric rotor which is parallel to one of the principal axes of the spacecraft. It will be supposed that one of the moments of inertia of the platform is a periodic function of time and that the center of mass of the spacecraft is not modified. Under these assumptions, it is shown that in the absence of external torques and spinning rotors the system possesses chaotic behavior in the sense that it exhibits Smale's horseshoes. We prove this statement by means of the Melnikov method.

The presence of chaotic behavior results in a random spin-up operation. This randomness is visualized by means of maps of the initial conditions with final nutation angle close to zero. This phenomenon is well described by a suitable parameter that measures the amount of randomness of the process. Finally, we relate this parameter with the Melnikov function in the absence of the spinning rotor and with the presence of subharmonic resonances.

1. Introduction

Basically, a dual-spin spacecraft, also called a gyrostat, is a mechanical system $\mathcal{G}$ composed by several bodies: a main rigid body $\mathcal{P}$, called platform or core body, and other axisymmetric bodies $\mathcal{R}$, called rotors or wheels. These rotors are not rigidly connected to the platform, but they can have a motion of relative rotation with respect to the platform, in such a way that the motion of the rotors does not modify the distribution of masses of the spacecraft. Thus, the gyrostat represents a model for a rotating body with an internal angular momentum.

This model has been used with success in the study of the dynamics of different physical systems since the end of the 19th century. Peano [1895a, 1895b] and Volterra [1899] applied the gyrostat model to the rotation of the Earth in order to explain the motion of its poles and the variation of the latitude on the surface of the Earth. They considered the Earth as a rigid body but with an internal angular momentum due to internal motions as the ocean currents. Later on, Kramers [1923], following Volterra's example, started to consider the effect of internal electronic angular momenta of molecules on their rotational spectra. Several theoretical results on the attitude dynamics of gyrostats in different particular situations have been collected in Leimanis's book [1965, pp. 207–238].

*E-mail: manuel.inarrea@dq.unirioja.es
†E-mail: vlancha@dmc.unirioja.es

In the last decades, the dynamics of the gyrostat has been the object of great interest in astrodynamics and space engineering, this is because nowadays most artificial satellites have one or more rotors in order to control the attitude and to stabilize the rotations of the spacecraft. So, the gyrostat is an useful model to study, at first approximation, the attitude dynamics of dual-spin spacecrafts [Hughes, 1986; Wiesel, 1997].

Moreover, the gyrostat model also matches with several problems in nuclear and atomic physics [Ring & Schuck, 1980; Elipe & Ferrer, 1994]; and with optical problems [David *et al.*, 1990].

Recently, many authors have studied different problems on gyrostats in various situations, most of them related to the dynamics of artificial satellites. Some of these authors have obtained analytical solutions of the equations of motion of free gyrostats [Cochran *et al.*, 1982, 1983] or under a central field [Cavas & Vigueras, 1994]. Other authors have focused on the attitude dynamics and the reorientation process of various types of gyrostats [Hubert, 1980; Hall & Rand 1994; Hall, 1995a, 1995b, 1995c, 1996, 1997]. On the other hand, several authors have used the Melnikov method in order to analyze the chaotic behavior of a gyrostat under different kinds of perturbations [Holmes & Marsden, 1983; Koiller, 1984; Tong *et al.*, 1995].

All these studies are based on the premise that the gyrostat is made of perfectly rigid components. Unfortunately, all real materials are elastic and deformable to some degree. The model of perfectly rigid components can lead to results not coincident with the real behavior of the spacecraft. This mistake was dramatically pointed out in 1958 when an unexpected instability appeared in the rotation of the Explorer I satellite [Thomson, 1986, pp. 212–213].

This consideration has moved us to focus our attention on the dynamics of a dual-spin spacecraft with one of the moments of inertia as a periodic function of time. The system is in the absence of external torques and the center of mass of the spacecraft is not modified. In this specific case, Lanchares *et al.* [1998] and Iñarrea [1998] have proved, using the Melnikov method, that the system exhibits chaotic motion and that it can be removed by means of a spinning rotor about one of the principal axes of the gyrostat. This model is a more realistic approximation to the attitude motion of a spacecraft than the perfectly rigid model, but not exempt from considerable simplifications.

Following several authors, we treat the problem in noncanonical variables: the components of the total angular momentum in the body frame. As Elipe *et al.* [1997] and Elipe and Lanchares [1997a, 1997b] have shown, in these variables the free gyrostat model reduces to a quadratic Hamiltonian with a spherical phase space, and so the phase flow can be easily interpreted. Besides, this kind of Hamiltonians has been widely studied in order to determine their equilibria, bifurcations and phase flow evolution [Lanchares & Elipe, 1995a, 1995b; Lanchares *et al.*, 1995].

The present paper is structured in the following way. In Sec. 2, we develop the Hamiltonian formulation corresponding to a generic free gyrostat with n rotors aligned in different directions. Then we focus on the particular case of a free triaxial gyrostat and treat its Hamiltonian as a sum of an integrable part plus a time-periodic perturbation. In Sec. 3, we calculate the Melnikov function of the perturbed system when the rotors are at relative rest. The Melnikov function gives us an analytical estimation of the width of the stochastic layer generated by the perturbation. In the next section, we analyze the dependence of this analytical estimation on the parameters of the perturbation. Also we check the validity of this analytical estimation calculating a numerical estimation of the width of the layer. We find some deviations between both estimations due to the effect of nonlinear resonances. In Sec. 5 we consider the reorientation process and the effect of the perturbation in it. In order to show the influence of the perturbation, a suitable parameter is introduced and it is related to the Melnikov function calculated in Sec. 3. Finally, in Sec. 6, we take into account the effect of nonlinear resonances to explain the sudden increments of the amount of apparent chaotic motion of the system.

2. Hamiltonian and Equations of Motion

Let us consider a gyrostat, consisting of an asymmetric platform and n axisymmetric rotors aligned in different directions. As the gyrostat is in the absence of external forces and torques, we can assume that the gyrostat has a fixed point O, identified with its center of mass. Centered on it we will use two orthonormal reference frames

— $\mathcal{S}$, the inertial space frame $O\mathbf{s}_1\mathbf{s}_2\mathbf{s}_3$ fixed in the space.

— $\mathcal{B}$, the body frame $O\mathbf{b}_1\mathbf{b}_2\mathbf{b}_3$ fixed in the platform. The directions of the orthogonal basis ($\mathbf{b}_1$, $\mathbf{b}_2$, $\mathbf{b}_3$) coincide with the principal axes of the gyrostat.

The relative orientation between these two reference frames results from three consecutive rotations involving the Euler angles (ψ, θ, ϕ) [Goldstein, 1992, pp. 183–188] (see Fig. 1).

Let $\mathbf{x} = x_1\mathbf{b}_1 + x_2\mathbf{b}_2 + x_3\mathbf{b}_3$ be the position vector of a generic particle P of the gyrostat with mass dm. The absolute velocity of this particle in the body frame $\mathcal{B}$ is

$$\mathbf{v}_{ab} = \frac{d\mathbf{x}}{dt} = \mathbf{v} + \boldsymbol{\omega} \times \mathbf{x}\,,$$

where $\mathbf{v} = \dot{x}_1\mathbf{b}_1 + \dot{x}_2\mathbf{b}_2 + \dot{x}_3\mathbf{b}_3$ is the relative velocity of P with respect to the platform, and $\boldsymbol{\omega}$ is the angular velocity vector of the body frame $\mathcal{B}$ with respect to the space frame $\mathcal{S}$. That is, $\boldsymbol{\omega}$ is the rotation angular velocity of the platform.

The angular momentum vector $\mathbf{dG}$ of the particle P with respect to the center of mass O in the body frame $\mathcal{B}$ is

$$\mathbf{dG} = \mathbf{x} \times \mathbf{dp} = \mathbf{x} \times \mathbf{v}_{ab}\, dm\,.$$

The gyrostat $\mathcal{G}$ can be considered as the union of the platform $\mathcal{P}$ plus the rotors $\mathcal{R}$, $\mathcal{G} = \mathcal{P} \cup \mathcal{R}$. With this and taking into account that $\mathbf{v} = 0$ for particles belonging to the platform, the total angular momentum $\mathbf{G}$ of the gyrostat in the body frame $\mathcal{B}$ can be expressed as

$$\begin{aligned}
\mathbf{G} &= G_x\mathbf{b}_1 + G_y\mathbf{b}_2 + G_z\mathbf{b}_3 \\
&= \int_{\mathcal{P}} [\mathbf{x} \times (\boldsymbol{\omega} \times \mathbf{x})] dm + \int_{\mathcal{R}} [\mathbf{x} \times (\mathbf{v} + \boldsymbol{\omega} \times \mathbf{x})] dm \\
&= \int_{\mathcal{P}} [\mathbf{x} \times (\boldsymbol{\omega} \times \mathbf{x})] dm + \int_{\mathcal{R}} [\mathbf{x} \times (\boldsymbol{\omega} \times \mathbf{x})] dm \\
&\quad + \int_{\mathcal{R}} (\mathbf{x} \times \mathbf{v}) dm \\
&= \int_{\mathcal{G}} [\mathbf{x} \times (\boldsymbol{\omega} \times \mathbf{x})] dm + \int_{\mathcal{R}} (\mathbf{x} \times \mathbf{v}) dm \\
&= \mathbb{I}\boldsymbol{\omega} + \mathbf{h}\,,
\end{aligned} \tag{1}$$

where $\mathbb{I} = \mathbb{I}_{\mathcal{P}} + \sum \mathbb{I}_{\mathcal{R}_i}$ is the tensor of inertia of the gyrostat, $\mathcal{G} = \mathcal{P} \cup \mathcal{R}$. As it is expressed in the body frame $\mathcal{B}$ of the principal axes of the gyrostat, this tensor is a diagonal one, that is, $\mathbb{I} = \mathrm{diag}(s_{11}, s_{22}, s_{33})$. On the other hand,

$$\mathbf{h} = h_x\mathbf{b}_1 + h_y\mathbf{b}_2 + h_z\mathbf{b}_3 = \int_{\mathcal{R}} (\mathbf{x} \times \mathbf{v}) dm\,,$$

is the relative angular momentum of the n rotors with respect to the platform.

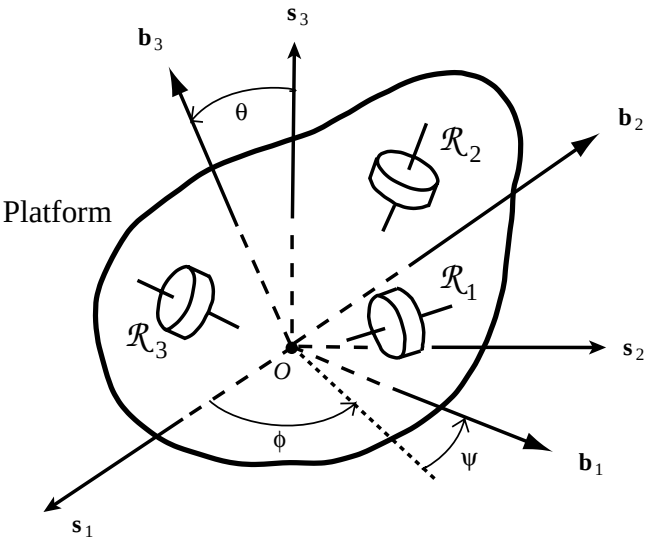

Fig. 1. Basic structure of a gyrostat with three attached rotors aligned in different directions.

In a similar way we obtain for the total kinetic energy of the gyrostat

$$\begin{aligned}
T &= \frac{1}{2}\int_{\mathcal{G}} \mathbf{v}_{ab}^2 dm = \frac{1}{2}\int_{\mathcal{G}} (\mathbf{v} + \boldsymbol{\omega} \times \mathbf{x})^2 dm \\
&= \frac{1}{2}\int_{\mathcal{G}} (\boldsymbol{\omega} \times \mathbf{x})^2 dm + \boldsymbol{\omega} \cdot \int_{\mathcal{R}} (\mathbf{x} \times \mathbf{v}) dm \\
&\quad + \frac{1}{2}\int_{\mathcal{R}} \mathbf{v}^2 dm \\
&= \frac{1}{2}\boldsymbol{\omega} \cdot \mathbb{I}\boldsymbol{\omega} + \mathbf{h} \cdot \boldsymbol{\omega} + T_{\mathcal{R}}\,,
\end{aligned} \tag{2}$$

where $T_{\mathcal{R}}$ represents the kinetic energy of the relative motion of the n rotors with respect to the platform.

As we consider a gyrostat in free rotation ($V = 0$), the Lagrangian $\mathcal{L}$ of the system is

$$\mathcal{L} = T - V = T = \frac{1}{2}\boldsymbol{\omega} \cdot \mathbb{I}\boldsymbol{\omega} + \mathbf{h} \cdot \boldsymbol{\omega} + T_{\mathcal{R}}\,. \tag{3}$$

As it is well known, the components (ω_x, ω_y, ω_z) of the angular velocity $\boldsymbol{\omega}$ in the body frame $\mathcal{B}$, can be written in terms of the Euler angles (ψ, θ, ϕ) and the Euler angles velocities ($\dot{\psi}$, $\dot{\theta}$, $\dot{\phi}$) as

[Goldstein, 1992, pp. 225–226]

$$\begin{cases} \omega_x = \dot{\phi}\sin\theta\sin\psi + \dot{\theta}\cos\psi\,, \\ \omega_y = \dot{\phi}\sin\theta\cos\psi - \dot{\theta}\sin\psi\,, \\ \omega_z = \dot{\phi}\cos\theta + \dot{\psi}\,. \end{cases} \tag{4}$$

Making use of these equations the Lagrangian $\mathcal{L}$ of the system could be explicitly expressed in terms of three generalized coordinates $\mathbf{q} = (\phi,\, \theta,\, \psi)$, and their velocities $\dot{\mathbf{q}} = (\dot{\phi},\, \dot{\theta},\, \dot{\psi})$.

The Hamiltonian $\mathcal{H}(\mathbf{q},\, \mathbf{p})$ is the Legendre transformations with respect to the velocities of the Lagrangian function $\mathcal{L}(\mathbf{q},\, \dot{\mathbf{q}})$

$$\mathcal{H}(\mathbf{q},\, \mathbf{p}) = \sum p_i\dot{q}_i - \mathcal{L}(\mathbf{q},\, \dot{\mathbf{q}})$$

where p_i is the canonically conjugate momentum, $p_i = \partial\mathcal{L}/\partial\dot{q}_i$.

In this case, the Lagrangian is expressible as the addition of three terms, $\mathcal{L} = \mathcal{L}_2 + \mathcal{L}_1 + \mathcal{L}_0$. The first term, $\mathcal{L}_2 = 1/2\boldsymbol{\omega}\cdot\mathbb{I}\boldsymbol{\omega}$, is a quadratic homogeneous function on the velocity $\dot{\mathbf{q}}$. The second term $\mathcal{L}_1 = \mathbf{h}\cdot\boldsymbol{\omega}$ is a linear homogeneous function on $\dot{\mathbf{q}}$, and the third term, $\mathcal{L}_1 = T_{\mathcal{R}}$ is a non-dependent function on $\dot{\mathbf{q}}$. So, by virtue of the Euler theorem for homogeneous functions, the Hamiltonian of the system is

$$\begin{aligned} \mathcal{H} = \nabla_{\dot{\mathbf{q}}}\mathcal{L}\cdot\dot{\mathbf{q}} - \mathcal{L} &= 2\mathcal{L}_2 + \mathcal{L}_1 - \mathcal{L}_2 - \mathcal{L}_1 - \mathcal{L}_0 \\ &= \mathcal{L}_2 - \mathcal{L}_0 = \frac{1}{2}\boldsymbol{\omega}\cdot\mathbb{I}\boldsymbol{\omega} - T_{\mathcal{R}}\,. \end{aligned} \tag{5}$$

Taking into account Eq. (1), this Hamiltonian can be expressed in terms of the total angular momentum $\mathbf{G}$ as

$$\mathcal{H} = \frac{1}{2}(\mathbf{G}-\mathbf{h})\cdot\mathbb{I}^{-1}(\mathbf{G}-\mathbf{h}) - T_{\mathcal{R}}\,. \tag{6}$$

As the components $(G_x,\, G_y,\, G_z)$ of the total angular momentum $\mathbf{G}$ in the body frame $\mathcal{B}$ are not canonical variables, it is necessary to know the Poisson brackets of these components G_i. The canonically conjugate momentum, p_i is

$$p_i = \frac{\partial\mathcal{L}}{\partial\dot{q}_i} = \mathbb{I}\boldsymbol{\omega}\cdot\frac{\partial\boldsymbol{\omega}}{\partial\dot{q}_i} + \mathbf{h}\cdot\frac{\partial\boldsymbol{\omega}}{\partial\dot{q}_i} = \mathbf{G}\cdot\frac{\partial\boldsymbol{\omega}}{\partial\dot{q}_i}\,. \tag{7}$$

By applying this equation, the components $(G_x,\, G_y,\, G_z)$ may be expressed in terms of the Euler angles $\mathbf{q} = (\phi,\, \theta,\, \psi)$ and their canonically conjugate momenta $\mathbf{p} = (p_\phi,\, p_\theta,\, p_\psi)$ as

$$\begin{cases} G_x = \left(\dfrac{p_\phi - p_\psi\cos\theta}{\sin\theta}\right)\sin\psi + p_\theta\cos\psi\,, \\ G_y = \left(\dfrac{p_\phi - p_\psi\cos\theta}{\sin\theta}\right)\cos\psi - p_\theta\sin\psi\,, \\ G_z = p_\psi\,. \end{cases} \tag{8}$$

Making use of these equations, it is just a matter of computing partial derivatives to obtain the Poisson brackets between the components G_i,

$$\begin{gathered} \{G_x;\, G_y\} = -G_z, \quad \{G_x;\, G_y\} = -G_x\,, \\ \{G_z;\, G_x\} = -G_y\,. \end{gathered} \tag{9}$$

From here on, we will consider the case of a gyrostat with three rotors aligned with the principal axes of the gyrostat, that is, the axes of the body frame $\mathcal{B}$. In this situation, denoting the x-axis rotor as rotor 1, the y-axis rotor as rotor 2, and the z-axis rotor as rotor 3, the angular velocities of each rotor can be written as

$$\begin{cases} \omega_1 = \boldsymbol{\omega} + \boldsymbol{\Omega}_1 = (\omega_x + \Omega_x,\, \omega_y,\, \omega_z)\,, \\ \omega_2 = \boldsymbol{\omega} + \boldsymbol{\Omega}_2 = (\omega_x,\, \omega_y + \Omega_y,\, \omega_z)\,, \\ \omega_3 = \boldsymbol{\omega} + \boldsymbol{\Omega}_3 = (\omega_x,\, \omega_y,\, \omega_z + \Omega_z)\,, \end{cases}$$

where $\boldsymbol{\Omega}_1 = (\Omega_x,\, 0,\, 0)$, $\boldsymbol{\Omega}_2 = (0,\, \Omega_y,\, 0)$ and $\boldsymbol{\Omega}_3 = (0,\, 0,\, \Omega_z)$, are the relative angular velocities of each rotor with respect to the platform.

Moreover, in this case the relative angular momentum $\mathbf{h}$ of the rotors can be calculated more explicitly

$$\begin{aligned} \mathbf{h} = \int_{\mathcal{R}}(\mathbf{x}\times\mathbf{v})dm &= \int_{\mathcal{R}_1}(\mathbf{x}\times\mathbf{v}_1)dm \\ &+ \int_{\mathcal{R}_2}(\mathbf{x}\times\mathbf{v}_2)dm + \int_{\mathcal{R}_3}(\mathbf{x}\times\mathbf{v}_3)dm\,, \end{aligned}$$

and since we can now write $\mathbf{v}_i = \boldsymbol{\Omega}_i\times\mathbf{x}$,

$$\mathbf{h} = \sum_{i=1}^{3}\int_{\mathcal{R}_i}[\mathbf{x}\times(\boldsymbol{\Omega}_i\times\mathbf{x})]dm = \sum_{i=1}^{3}\mathbb{I}_{\mathcal{R}_i}\boldsymbol{\Omega}_i\,,$$

where $\mathbb{I}_{\mathcal{R}_i}$ is the tensor of inertia of the $\mathcal{R}_i$ rotor. It is a diagonal tensor in the body frame $\mathcal{B}$, that is, $\mathbb{I}_{\mathcal{R}_i} = \mathrm{diag}(A_{i11},\, A_{i22},\, A_{i33})$.

Thus, we obtain

$$\begin{aligned} \mathbf{h} = h_x\mathbf{b}_1 + h_y\mathbf{b}_2 + h_z\mathbf{b}_3 &= A_{111}\Omega_x\,\mathbf{b}_1 \\ &+ A_{222}\Omega_y\,\mathbf{b}_2 + A_{333}\Omega_z\,\mathbf{b}_3\,, \end{aligned}$$

where h_i now represents the relative angular momentum of each individual rotor with respect to the platform.

On the other hand, in this situation the kinetic energy $T_{\mathcal{R}}$ of the relative motion of the rotors can be expressed in a more explicit form

$$\begin{aligned} T_{\mathcal{R}} &= \frac{1}{2}\int_{\mathcal{R}} \mathbf{v}^2 dm = \frac{1}{2}\sum_{i=1}^{3}\int_{\mathcal{R}_i} \mathbf{v}_i^2 dm = \frac{1}{2}\sum_{i=1}^{3}\int_{\mathcal{R}_i} (\mathbf{\Omega}_i \times \mathbf{x})^2 dm \\ &= \frac{1}{2}\sum_{i=1}^{3} \mathbf{\Omega}_i \cdot \mathbb{I}_{\mathcal{R}_i}\mathbf{\Omega}_i = \frac{1}{2}(A_{111}\Omega_x^2 + A_{222}\Omega_y^2 + A_{333}\Omega_z^2) \\ &= \frac{1}{2}\left(\frac{h_x^2}{A_{111}} + \frac{h_y^2}{A_{222}} + \frac{h_z^2}{A_{333}}\right). \end{aligned}$$

Thus, and taking into account that in the body frame $\mathbb{I}^{-1}$ is also a diagonal tensor, in this case the Hamiltonian (6) results

$$\begin{aligned} \mathcal{H} = \frac{1}{2}&\left(\frac{G_x^2}{s_{11}} + \frac{G_y^2}{s_{22}} + \frac{G_z^2}{s_{33}}\right) - \left(\frac{G_x h_x}{s_{11}} + \frac{G_y h_y}{s_{22}} + \frac{G_z h_z}{s_{33}}\right) \\ &+ \frac{1}{2}\left(\frac{h_x^2}{s_{11}} + \frac{h_y^2}{s_{22}} + \frac{h_z^2}{s_{33}}\right) - \frac{1}{2}\left(\frac{h_x^2}{A_{111}} + \frac{h_y^2}{A_{222}} + \frac{h_z^2}{A_{333}}\right). \end{aligned} \tag{10}$$

Note that there is no loss of generality in considering the case of the rotors aligned with the principal axes of the gyrostat, because of the Hamiltonian of the system is always in the form of Eq. (10), even if the rotors are not aligned with the principal axes. However, in that case (h_x, h_y, h_z) do not represent the individual relative angular momentum of any particular rotor, but they are the components of the relative angular momentum of the rotors set.

The Poisson brackets (9) yields the Eulerian equations of motion for Hamiltonian (10)

$$\begin{aligned} \dot{G}_x &= \{G_x;\, \mathcal{H}\} = \left(\frac{1}{s_{33}} - \frac{1}{s_{22}}\right) G_y\, G_z + \frac{h_y}{s_{22}} G_z - \frac{h_z}{s_{33}} G_y\,, \\ \dot{G}_y &= \{G_y;\, \mathcal{H}\} = \left(\frac{1}{s_{11}} - \frac{1}{s_{33}}\right) G_x\, G_z - \frac{h_x}{s_{11}} G_z + \frac{h_z}{s_{33}} G_x\,, \\ \dot{G}_z &= \{G_z;\, \mathcal{H}\} = \left(\frac{1}{s_{22}} - \frac{1}{s_{11}}\right) G_x\, G_y + \frac{h_x}{s_{11}} G_y - \frac{h_y}{s_{22}} G_x\,. \end{aligned} \tag{11}$$

The Hamiltonian (10) is invariant under the group SO(2) of rotations $R(\phi, \mathbf{s}_3)$ about the space axis $\mathbf{s}_3$, since the angle ϕ is ignorable in $\mathcal{H}$ as it can be checked by replacing Eqs. (8) into (10).

On the other hand, by virtue of the angular momentum theorem and as we are considering a gyrostat in free motion, the total angular momentum $\mathbf{G}$ is constant in the space frame $\mathcal{S}$, and consequently its norm G is also constant. Therefore, the problem is also invariant under the group SO(3) of rotations about the origin O. As it is well known, the change from the space frame $\mathcal{S}$ to the body frame $\mathcal{B}$ may be directly done by means of one rotation. Thus, as the norm of a vector is invariant under the action of de SO(3) group, the norm G of the total angular momentum $\mathbf{G}$ is also constant in the body frame $\mathcal{B}$, that is, $G = \sqrt{G_x^2 + G_y^2 + G_z^2} =$ cte. It can also be easily checked by making use of Eq. (9), since

$$\dot{G} = \frac{1}{G}(G_x \cdot G_x + G_y \cdot G_y + G_z \cdot G_z) = 0\,.$$

Therefore, in the noncanonical variables (G_x, G_y, G_z), the phase space of the system may be regarded as a foliation of invariant manifolds

$$S^2(G) = \{(G_x,\, G_y,\, G_z) | G_x^2 + G_y^2 + G_z^2 = G^2\}\,.$$

The total angular momentum $\mathbf{G}$ in the body frame $\mathcal{B}$ describes a curve on the S^2 sphere of radius G. And the trajectories in the phase space are the level contours of the Hamiltonian (10) onto the sphere $S^2(G)$.

Making a scale change in the variables G_i, momenta h_i, and the time t, it is possible to reduce the phase space to a unique sphere of unit radius. So, if we define

$$\overline{G}_i = \frac{G_i}{G}, \quad \overline{h}_i = \frac{h_i}{G}, \quad \tau = Gt\,,$$

results $\overline{G}_x^2 + \overline{G}_y^2 + \overline{G}_z^2 = 1$ and

$$\{\overline{G}_x;\, \overline{G}_y\} = -\frac{\overline{G}_z}{G}, \quad \{\overline{G}_y;\, \overline{G}_z\} = -\frac{\overline{G}_x}{G}$$

$$\{\overline{G}_z;\, \overline{G}_x\} = -\frac{\overline{G}_y}{G}\,.$$

In this way, the equations of motion and the Hamiltonian of the system do not change their forms of Eqs. (11) and (10). In order to simplify the notation, from here on we will omit the bars and denote the time variable τ as t.

On the other hand, as we will suppose, from here on, that the quantities s_{jj}, $\bar{h}_j$ and A_{jjj} are known functions of time, the dynamics of the problem is defined by the reduced Hamiltonian

$$\mathcal{H} = \frac{1}{2}\left(\frac{G_x^2}{s_{11}} + \frac{G_y^2}{s_{22}} + \frac{G_z^2}{s_{33}}\right) - \left(\frac{G_x h_x}{s_{11}} + \frac{G_y h_y}{s_{22}} + \frac{G_z h_z}{s_{33}}\right). \qquad (12)$$

The Hamiltonian (12) belongs to the kind of quadratic Hamiltonians with SU(2) algebraic structure on the unit sphere S^2. This kind of Hamiltonians may be reduced by means of equivalence transformations to six different generic types depending on the essential parameters of the problem [Frauendiener, 1995]. This kind of quadratic Hamiltonians has been widely studied in order to determine their equilibria, bifurcations and phase flow evolution in terms of the parameters of the Hamiltonian [Lanchares & Elipe, 1995a, 1995b; Lanchares *et al.*, 1995].

Note that the topology of the phase space remains unchanged even if the moments of inertia are functions of time, that is the kind of perturbation that we deal with in this paper. In particular, we consider a platform with one of its moments of inertia as a periodic function of time. So if we denote with $\mathbb{I}_{\mathcal{P}}$ the tensor of inertia of the platform, $\mathbb{I}_{\mathcal{P}}$ is a diagonal tensor in the body frame $\mathcal{B}$, that is, $\mathbb{I}_{\mathcal{P}} = \mathrm{diag}(A, B, C)$ since the rotors are aligned with the principal axes of the gyrostat. We will consider a triaxial platform with the relation $A > B > C$. We will suppose specifically that the greatest moment of inertia of the platform is a periodic function of time, that is, $A = A(t)$ whereas the two other moments of inertia, B and C remain constant. Although A varies with time, we will suppose that the platform always holds the same triaxial condition, $A(t) > B > C$, at any time. Also we will suppose that the center of mass of the gyrostat is not altered.

It is important to note that the choice of the greatest moment of inertia as function of time, and the other two constant, is not relevant in the dynamics of the problem. In fact, the results and conclusions are similar no matter what moment of inertia is supposed to be variable with time.

On the other hand, from here on we will suppose that the three rotors are perfectly rigid, that is, A_{ijj} = constant, and therefore the relative angular momenta h_j of the rotors are not affected by the elasticity of the platform.

The function that defines the change of the platform's greatest moment of inertia $A(t)$ is supposed to have the specific form

$$\frac{1}{s_{11}(t)} = \frac{1}{A(t) + A_{111} + A_{211} + A_{311}} = a_1(t) = a_{10} + \varepsilon\cos\nu t\,, \qquad (13)$$

where ε is a parameter much smaller than a_{10}, ($\varepsilon \ll a_{10}$). That is, $a_1(t)$ is a periodic function with frequency ν and amplitude ε. In this way, the dynamics of the problem is described by this Hamiltonian

$$\mathcal{H} = \frac{1}{2}(a_{10}G_x^2 + a_2 G_y^2 + a_3 G_z^2) - (a_{10}G_x h_x + a_2 G_y h_y + a_3 G_z h_z) + \left(\frac{1}{2}G_x^2 - G_x h_x\right)\varepsilon\cos\nu t\,, \qquad (14)$$

where $a_2 = 1/s_{22}$ and $a_3 = 1/s_{33}$.

Note that in the Hamiltonian (14) of the perturbed problem, there are two limit cases in which the problem is integrable: for $\nu = 0$, and for $\nu \to \infty$.

For $\nu \to \infty$, the problem is integrable because in this limit, the period T of the perturbation $(\varepsilon G_x^2 \cos\nu t)/2$ is zero, $T = 0$. This means that, although $a_1(t)$ is changing, it spends no time, $T = 0$, to make a complete oscillation. So, in this case the perturbation takes the constant value $\varepsilon G_x^2/2$, that

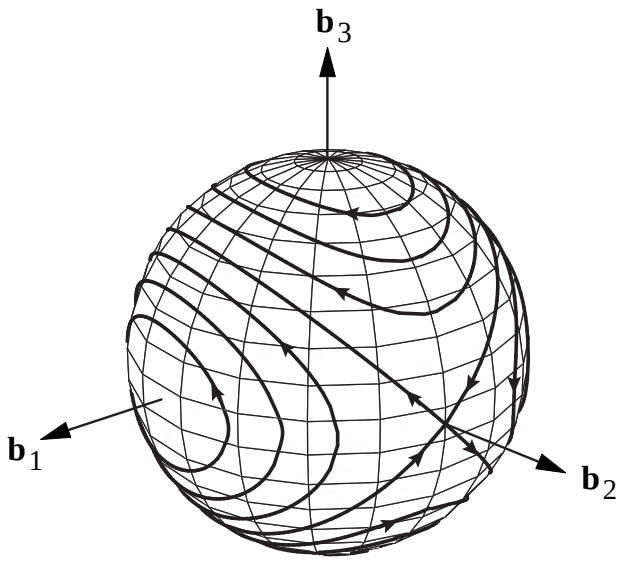

Fig. 2. The phase flow for the triaxial rigid body in free rotation ($a_{10} < a_2 < a_3$).

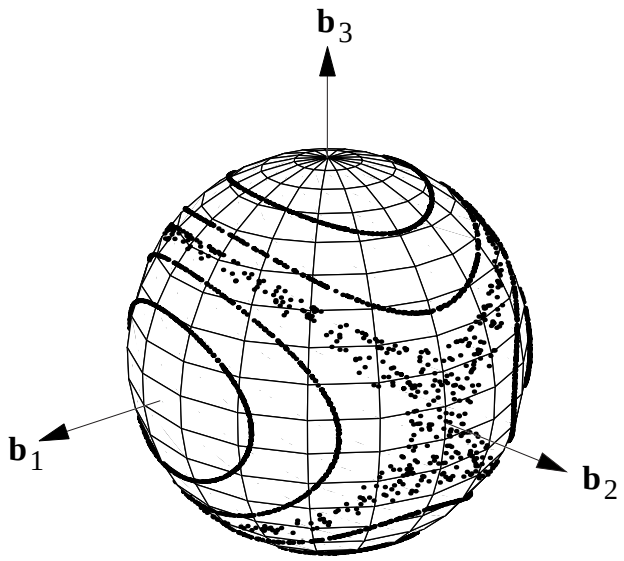

Fig. 3. Poincaré surface of section for $a_{10} = 0.1$, $a_2 = 0.2$, $a_3 = 0.3$, $\varepsilon = 0.005$ and $\nu = 0.1$.

is, the perturbation value for $t = 0$. Therefore, in the limit $\nu \to \infty$, the perturbed problem reduces to the integrable case of a quadratic Hamiltonian. On the other hand, in the case $\nu = 0$, the problem is also integrable. In this case, the perturbation is not a function of time, but a constant $\varepsilon G_x^2/2$. So, for $\nu = 0$, the perturbed problem also coincides with the integrable case of a quadratic Hamiltonian.

3. Rotors at Relative Rest. Chaotic Motion

The natural starting point in the study of the dynamics of the gyrostat described by the Hamiltonian (14) is to consider the three rotors at relative rest with respect to the platform, that is, $h_x = h_y = h_z = 0$. Under these conditions, the Hamiltonian of the system is

$$\mathcal{H} = \frac{1}{2}(a_{10}G_x^2 + a_2 G_y^2 + a_3 G_z^2) + \frac{1}{2}G_x^2 \varepsilon \cos \nu t$$
$$= \mathcal{H}_0 + \varepsilon V(G_x, G_y, G_z; t) \qquad (15)$$

where we will suppose that $a_1(t) < a_2 < a_3$, since $A(t) > B > C$.

Therefore, the Hamiltonian of the gyrostat may be expressed as a sum of an integrable term, $\mathcal{H}_0$, plus a time-periodically perturbation, $\varepsilon V(G_x, G_y, G_z; t)$, with period $T = 2\pi/\nu$. The integrable term, $\mathcal{H}_0$, is that of a triaxial rigid body with moments of inertia $1/a_{10} > 1/a_2 > 1/a_3$ in free motion.

We will apply the Melnikov method in order to prove that the problem shows chaotic behavior. For the application of this method it is necessary to know previously the solutions of the homo/heteroclinic trajectories of the unperturbed Hamiltonian $\mathcal{H}_0$.

Taking into account Eqs. (9) it is easy to obtain the well-known Eulerian equations of motion of the free rigid body.

$$\dot{G}_x = \{G_x; \mathcal{H}_0\} = (a_3 - a_2) G_y G_z \,,$$
$$\dot{G}_y = \{G_y; \mathcal{H}_0\} = (a_{10} - a_3) G_x G_z \,,$$
$$\dot{G}_z = \{G_z; \mathcal{H}_0\} = (a_2 - a_{10}) G_x G_y \,. \qquad (16)$$

From these equations, it is also easy to deduce that there are six equilibria located at the intersections of the body frame axes with the sphere S^2. The two equilibria located at the axis $\mathbf{b}_2$, of intermediate moment of inertia are unstable equilibria, whereas the other four equilibria are stable. The two unstable equilibria, denoted by E_1 and E_2, are connected by four heteroclinic trajectories. These orbits are the separatrices of the phase space. Figure 2 shows the main features of the phase flow for the triaxial rigid body in free rotation.

The four heteroclinic orbits are obtained for the Hamiltonian value $a_2/2$, the Hamiltonian value at the unstable equilibria. These separatrices divide the phase space into two different classes of motion: circulations about the axis $\mathbf{b}_1$ of maximal moment of inertia when $a_{10} < 2\mathcal{H}_0 < a_2$; and circulations

about the axis $\mathbf{b}_3$ of minimal moment of inertia when $a_2 < 2\mathcal{H}_0 < a_3$.

The explicit expressions of the different types of trajectories are obtained in terms of elliptic and hyperbolic functions, from Eqs. (16) by means of the two integrals $\mathcal{H}_0$ and G (for more details see [Deprit & Elipe, 1993]).

3.1. *Circulations about the axis of maximal moment of inertia*

In this case $a_{10} < 2\mathcal{H}_0 < a_2$ and the solutions are

$$\begin{aligned} G_x &= \Gamma_1 \mathrm{dn}(n_1 t,\, k_1)\,, \\ G_y &= \Gamma_2 \mathrm{sn}(n_1 t,\, k_1)\,, \\ G_z &= \Gamma_3 \mathrm{cn}(n_1 t,\, k_1)\,, \end{aligned} \tag{17}$$

where

$$\Gamma_1 = \sqrt{\frac{a_3 - 2\mathcal{H}_0}{a_3 - a_{10}}}, \quad \Gamma_2 = \sqrt{\frac{2\mathcal{H}_0 - a_{10}}{a_2 - a_{10}}}\,,$$

$$\Gamma_3 = \sqrt{\frac{2\mathcal{H}_0 - a_{10}}{a_3 - a_{10}}}$$

and

$$n_1 = \sqrt{(a_2 - a_{10})(a_3 - 2\mathcal{H}_0)}\,,$$

$$k_1^2 = \frac{(2\mathcal{H}_0 - a_{10})(a_3 - a_2)}{(a_2 - a_{10})(a_3 - 2\mathcal{H}_0)}\,.$$

3.2. *Circulations about the axis of minimal moment of inertia*

Now, $a_2 < 2\mathcal{H}_0 < a_3$ and the solutions are

$$\begin{gathered} G_x = \Gamma_1 \mathrm{cn}(n_3 t,\, k_3), \quad G_y = \gamma_2 \mathrm{sn}(n_3 t,\, k_3)\,, \\ G_z = \Gamma_3 \mathrm{dn}(n_3 t,\, k_3) \end{gathered} \tag{18}$$

where

$$\gamma_2 = \sqrt{\frac{a_3 - 2\mathcal{H}_0}{a_3 - a_2}}, \quad n_3 = \sqrt{(2\mathcal{H}_0 - a_{10})(a_3 - a_2)}$$

$$k_3 = \frac{1}{k_1}\,.$$

3.3. *Asymptotic orbits (heteroclinic trajectories)*

When $2\mathcal{H}_0 = a_2$, the four different asymptotic solutions, corresponding to the heteroclinic trajectories, are

$$\begin{cases} G_x = (-1)^{[(k-1)/2]} \sqrt{\dfrac{a_3 - a_2}{a_3 - a_{10}}}\, \mathrm{sech}(n_2 t)\,, \\ G_y = (-1)^{k-1} \tanh(n_2 t)\,, \qquad k = 1,\, 2,\, 3,\, 4\,. \\ G_z = (-1)^{[k/2]} \sqrt{\dfrac{a_2 - a_{10}}{a_3 - a_{10}}}\, \mathrm{sech}(n_2 t) \end{cases} \tag{19}$$

where

$$n_2 = \sqrt{(a_2 - a_{10})(a_3 - a_2)} \tag{20}$$

and $[b]$ stands for the integer part of b.

The four heteroclinic trajectories form the stable manifolds $W_s(E_1)$, $W_s(E_2)$ and the unstable ones $W_u(E_1)$, $W_u(E_2)$ corresponding to the two unstable equilibria. In the unperturbed problem the stable manifold of E_1 and the unstable manifold of E_2 join smoothly together, and vice versa, so it holds that $W_s(E_1) = W_u(E_2)$ and $W_u(E_1) = W_s(E_2)$. But if there exists a perturbation, these manifolds are not forced to coincide and it is possible that they intersect transversaly leading to an infinite number of new heteroclinic points. Then, a heteroclinic tangle is generated. In this case, because of the perturbation, the motion of the gyrostat near the separatrices becomes chaotic in the sense that the system exhibits Smale's horseshoes and a stochastic layer appears near the separatrices. Inside this chaotic layer small isolated regions of regular motion with periodic orbits can also appear.

The existence of heteroclinic intersections in the perturbed problem, and so the existence of chaotic motion, may be proved, at first order, by means of the Melnikov method [Guckenheimer & Holmes, 1983]. The Melnikov function, $M(t_0)$, for the Hamiltonian (15) is given by

$$M(t_0) = \int_{-\infty}^{\infty} \{\mathcal{H}_0(G_i(t - t_0));\, \varepsilon V(G_i(t - t_0),\, t)\}\, dt$$

$$i = x,\, y,\, z\,.$$

where G_i are precisely the solutions of the unperturbed heteroclinic orbits (19). The Poisson bracket $\{\mathcal{H}_0;\, \varepsilon V\}$ can be evaluated taking into account the structural identities (9) and we obtain

$$\{\mathcal{H}_0;\, \varepsilon V\} = (a_2 - a_3)\varepsilon G_x G_y G_z \cos \nu t\,. \qquad (21)$$

So, the Melnikov function results in

$$M(t_0) = \varepsilon \int_{-\infty}^{\infty} (a_2 - a_3) G_x G_y G_z \cos \nu t\, dt\,. \qquad (22)$$

By substitution of (19) into (22) we get

$$M(t_0) = \varepsilon \frac{(a_2 - a_3) n_2}{(a_3 - a_{10})} \int_{-\infty}^{\infty} \frac{\sinh[n_2(t - t_0)]}{\cosh^3[n_2(t - t_0)]} \cos \nu t\, dt\,. \qquad (23)$$

Integrating by parts we arrive at an integral that is tabulated by Gradshteyn and Ryzhik [1980, p. 505] and it finally results in

$$M(t_0) = \frac{(a_3 - a_2)\varepsilon \pi \nu^2}{2(a_3 - a_{10}) n_2^2 \sinh\left(\dfrac{\pi \nu}{2n_2}\right)} \sin \nu t_0 = \Delta\mathcal{H}(\varepsilon,\, \nu) \sin \nu t_0\,. \qquad (24)$$

We can conclude from (24) that the Melnikov function, $M(t_0)$, has simple zeroes for $\nu t_0 = k\pi$ with $k = 0,\, 1,\, 2, \ldots$ Therefore the perturbation produces heteroclinic intersections between the stable and unstable manifolds of the equilibria E_1 and E_2. So, the perturbation generates a layer of chaotic motion surrounding the unperturbed separatrices.

It is important to notice that a formula similar to (24) is obtained if any other moment of inertia of the platform (minimal or intermediate one) is supposed to be variable with time.

4. Estimation of the Width of the Stochastic Layer

In the previous section, we have seen that the perturbed system shows chaotic behavior whatever moment of inertia varies with time, in the sense that it appears as a layer of stochastic motion near the separatrices of the unperturbed problem. It is important to estimate the width of this layer in order to know the amount of apparent chaotic motion of the perturbed gyrostat and also the set of initial conditions with nonregular behavior. In this section we focus on the case in which only the maximal moment of inertia $A(t)$ is a function of time. The factor $\Delta\mathcal{H}$ that appears in Eq. (24)

$$\Delta\mathcal{H}(\varepsilon,\, \nu) = \frac{(a_3 - a_2)\varepsilon \pi \nu^2}{2(a_3 - a_{10}) n_2^2 \sinh\left(\dfrac{\pi \nu}{2n_2}\right)}\,, \qquad (25)$$

give us an analytical estimation [Zaslavsky *et al.*, 1991] of the Hamiltonian value in the border of the stochastic layer. According to Eq. (25) the width of the layer, in terms of the Hamiltonian value, is a function of the amplitude ε and frequency ν of the perturbation. Note, that fixed the frequency ν the width of the layer is a linear function of the amplitude ε and the bigger ε is the wider is the layer. On the other hand, fixed the amplitude ε, the width of the layer grows, as a function of ν, until it reaches a maximum value and then decreases asymptotically to zero. This behavior is plotted in Fig. 4 for $a_{10} = 0.1$, $a_2 = 0.2$ and $a_3 = 0.3$, and for (a) a fixed frequency $\nu = 0.3$ and (b) a fixed amplitude $\varepsilon = 0.01$.

The chaotic behavior of the gyrostat near the unperturbed separatrices may be observed by means of a Poincaré surface of section. The surface consists of time sections $t = \text{cte.}(\text{mod } T)$ of the fourth-dimensional $(G_x,\, G_y,\, G_z,\, t)$ extended phase space. Figure 3 shows the presence of a stochastic layer around the unperturbed separatrices. As it can be seen in this figure, the regular trajectories appear as closed curves, whereas chaotic ones appears like a cloud of points around the separatrices of the unperturbed problem.

To check the validity of the analytical estimation (25) of the width of the stochastic layer, a numerical estimation is needed. The basis in order to design the algorithm to estimate numerically the width of the layer is the following reasoning on the phase flow on S^2. Note that in the unperturbed problem, all the trajectories passing through the meridian $G_x = 0$, lie either on the northern hemisphere ($G_z > 0$) or on the southern one ($G_z < 0$). On the other hand, in the perturbed problem, the chaotic trajectories cover the stochastic layer, so that for these orbits the component G_z takes both positive and negative values. Therefore, we can consider as regular a trajectory which lies always in the same hemisphere, whereas we may consider as chaotic a trajectory crossing the equator $G_z = 0$.

Taking into account this consideration, for given values of ε and ν, we have swept the meridian

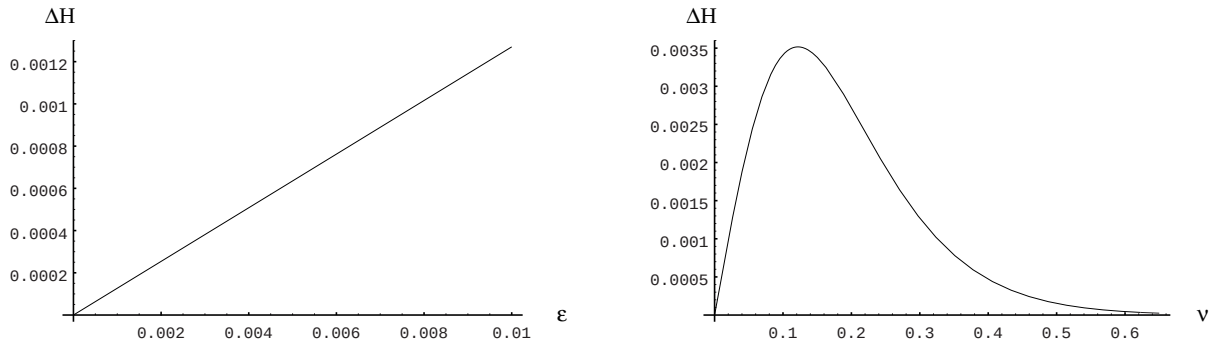

(a) (b)

Fig. 4. Evolution of the analytical estimation $\Delta\mathcal{H}(\varepsilon, \nu)$ of the width of the stochastic layer. (a) As a function of the amplitude ε, for $\nu = 0.3$. (b) As a function of the frequency ν, for $\varepsilon = 0.01$. In both cases $a_{10} = 0.1$, $a_2 = 0.2$ and $a_3 = 0.3$.

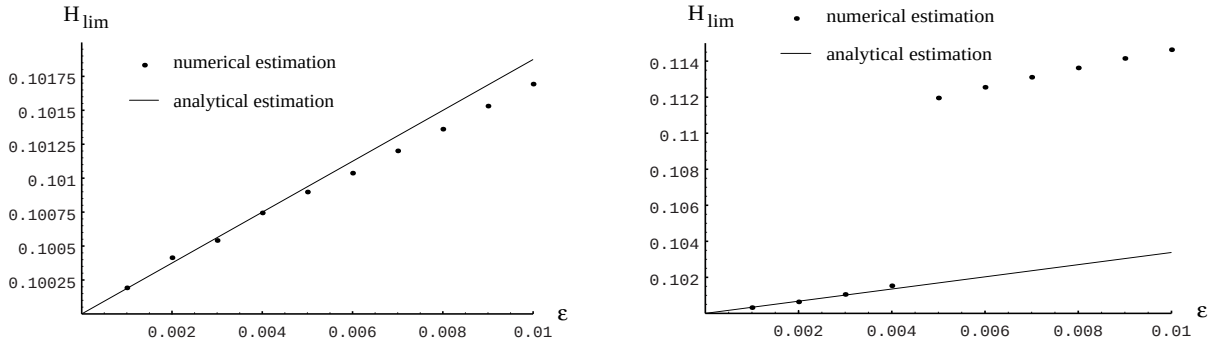

(a) (b)

Fig. 5. Comparative evolution of the estimations of the width of the stochastic layer as a function of the amplitude ε for two different fixed frequencies: (a) $\nu = 0.04$, and (b) $\nu = 0.15$. In both cases $a_{10} = 0.1$, $a_2 = 0.2$ and $a_3 = 0.3$.

$G_x = 0$ from $G_z = 1$ to $G_z = 0$ looking for the initial conditions of the first orbit passing through the equator to the southern hemisphere. Each orbit has been obtained by numerical integration of the equations of the motion

$$\dot{G}_x = \{G_x;\, \mathcal{H}\} = (a_3 - a_2) G_y\, G_z$$

$$\dot{G}_y = \{G_x;\, \mathcal{H}\} = (a_{10} - a_3 + \varepsilon \cos \nu t) G_x\, G_z$$

$$\dot{G}_z = \{G_x;\, \mathcal{H}\} = (a_2 - a_{10} - \varepsilon \cos \nu t) G_x\, G_y\,.$$

using a Runge–Kutta algorithm of fifth order with fixed step [Lambert, 1976, pp. 121–123], checking that the norm of the total angular momentum is "constant", that is, $G_x^2 + G_y^2 + G_z^2 = 1$. The orbits have been propagated 1000 periods of the perturbation and the initial condition of the first chaotic orbit has been calculated with a precision of 10^{-3}. This orbit determines the border of the layer and it allows us to calculate the width of it. With the initial conditions $(0,\, G_y,\, G_z)$ of this limit trajectory we can calculate the Hamiltonian value $\mathcal{H}_{\lim}$ of the perturbed problem at the initial instant $t = 0$, corresponding to the northern border of the layer at the meridian $G_x = 0$.

At this point, it is interesting to compare the analytical (25) and the numerical estimations of the width of the layer as functions of the amplitude ε and the frequency ν of the perturbation. Figures 5 and 6 show in a comparative way, the analytical and the numerical estimations of the value $\mathcal{H}_{\lim}$ at the northern border of the layer. We have calculated the analytical estimation of $\mathcal{H}_{\lim}$ as $\mathcal{H}_{\lim} = \mathcal{H}_s + \Delta\mathcal{H}$, where $\mathcal{H}_s = a_2/2$ is the Hamiltonian value at the unperturbed separatrices, and $\Delta\mathcal{H}$ is the analytical estimation (25) of the width of the layer. In these three plots we have considered a gyrostat with $a_{10} = 0.1, a_2 = 0.2$ and $a_3 = 0.3$. Figure 5 presents the evolution of both estimations of $\mathcal{H}_{\lim}$ as a function of the amplitude ε for two different constant frequencies. The values of ε vary from 0.001 to 0.01 with steps of 0.001. On the other hand,

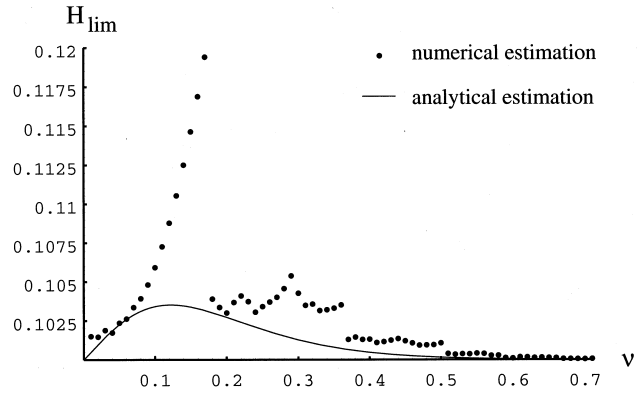

Fig. 6. Comparative evolution of the estimations of the width of the stochastic layer as a function of the frequency ν for a fixed amplitude $\varepsilon = 0.01$, and for $a_{10} = 0.1$, $a_2 = 0.2$ and $a_3 = 0.3$.

Fig. 6 shows the comparative evolution of the estimations of $\mathcal{H}_{\rm lim}$ as functions of ν, for a fixed amplitude value $\varepsilon = 0.01$. The frequency ν, varies from 0.01 to 0.7 with steps of 0.01.

As it can be seen in Fig. 5(a) for a low fixed value of the frequency $\nu = 0.04$, there exists a great agreement between the analytical and numerical estimations. Thus, the predicted behavior of Eq. (25) is confirmed by the numerical estimation: For a fixed frequency, the width of the layer grows linearly with the amplitude ε of the perturbation. In Fig. 5(b) it can be observed that for an intermediate frequency value $\nu = 0.15$, the numerical estimation is very close to the analytical one for small values of the amplitude $\varepsilon \leq 0.004$. Nevertheless, between

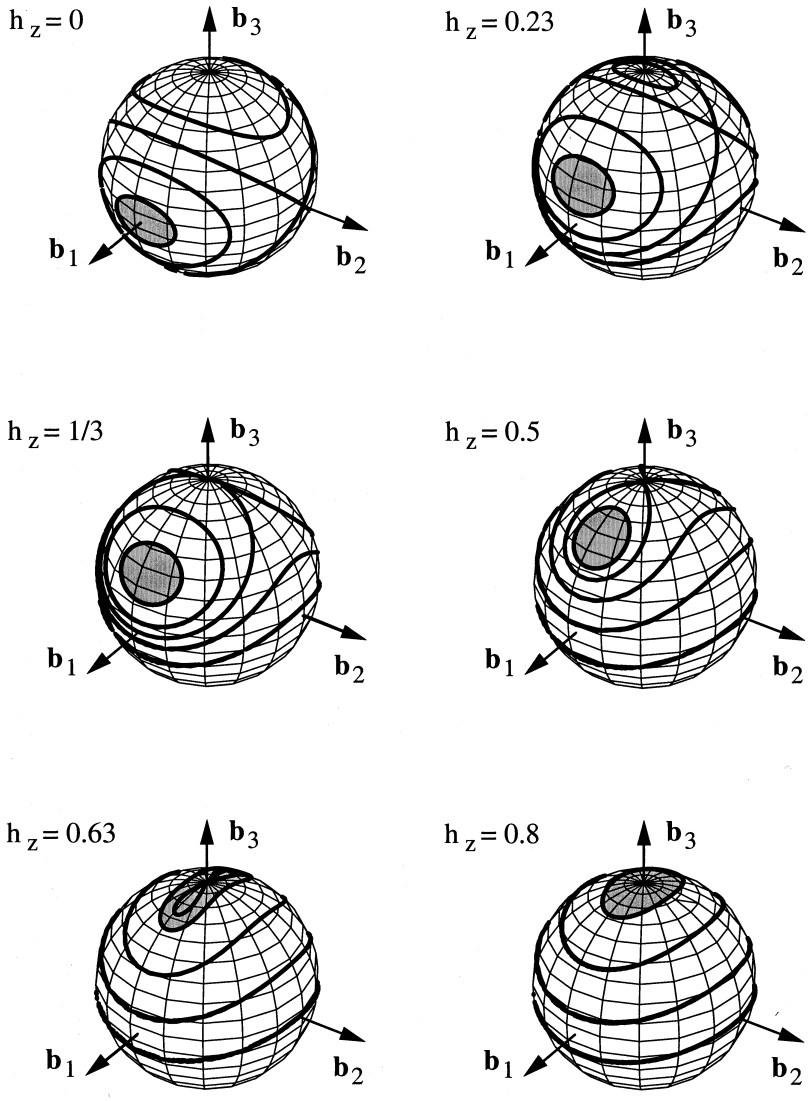

Fig. 7. Evolution of the phase space of the unperturbed gyrostat as h_z increases. In gray, the region of initial conditions with a final nutation angle $\theta < 20^\circ$. $a_{10} = 0.1$, $a_2 = 0.2$ and $a_3 = 0.3$.

the values $\varepsilon = 0.004$ and $\varepsilon = 0.005$, a sharp increase of the numerical estimation of $\mathcal{H}_{\lim}$ stands out, so that, for values $\varepsilon \geq 0.005$, the numerical estimation is always rather greater than the analytical one.

As we will explain in Sec. 6, these abrupt increases of the numerical estimations, not reflected in the analytical estimation, are due to the fact that the stochastic layer engulfs a nonlinear resonance.

Figure 6 reveals the two integrable limits of the perturbed problem: for $\nu = 0$, and for $\nu \to \infty$. It may be observed that for high values of the frequency, as ν grows, the $\mathcal{H}_{\lim}$ value tends asymptotically to zero, that is, the stochastic layer tends to disappear in the integrable limit for $\nu \to \infty$. On the other hand, for frequency values close to zero, as ν decreases the $\mathcal{H}_{\lim}$ value tends to zero, and so the layer also tends to disappear in the other integrable limit for $\nu = 0$.

Figure 6 also shows some abrupt increases in the evolution of the numerical estimation of $\mathcal{H}_{\lim}$, e.g. for $\nu = 0.18$ or $\nu = 0.37$, resulting in great differences between both estimations for intermediate frequency values. The explanation of these differences is essentially the same that we have given before. For certain values of ν, there are nonlinear resonances near the border of the stochastic layer, either inside of it or outside of it. The size of these resonances depends strongly on the frequency ν, increasing, decreasing or even disappearing suddenly as ν varies. This fact affects the evolution of the border of the layer producing those sharp changes of the numerical estimation observed in Figs. 5(b) and 6.

5. The Effect of the Perturbation in the Reorientation Process

As we have indicated above, the study of the gyrostat dynamics has an important application in the attitude control and the rotation stabilization of the spacecrafts. Almost all spacecrafts need to maintain a constant orientation with respect to an inertial space frame $\mathcal{S}\{O\mathbf{s}_1\mathbf{s}_2\mathbf{s}_3\}$, because of pointing requirements for antennas, cameras or solar-panels. Among the various techniques used for this requirement, the simplest one is based on the principle of conservation of the total angular momentum $\mathbf{G}$ of the vehicle. If the spacecraft has sufficiently large total angular momentum and it is free of external torques, or if they are very small, the angular momentum vector $\mathbf{G}$ of the system will remain essentially constant both in magnitude and direction.

It is important to point out that the noncanonical formalism we use is very useful in order to describe this process, as several authors [Hubert, 1980; Krishnaprasad, 1985; Hall, 1995a] have stated it before. Moreover, this formulation allows to explain in a simple way, more complex processes like momentum transfer [Hall, 1996, 1997] or resonance captures [Hall, 1995b], that are directly related to the reorientation process.

For a free gyrostat, the total angular momentum $\mathbf{G}$ is constant in the space frame $\mathcal{S}$, but in this frame the gyrostat orientation can change with time due to precessional and nutational motions around the fixed direction of $\mathbf{G}$. This variation of the attitude is reflected by the trajectories of the total angular momentum vector $\mathbf{G}$ in the spherical phase space constructed in the body frame $\mathcal{S}$ (see Fig. 2 for rotor at rest), as in that frame the gyrostat orientation is fixed and the vector $\mathbf{G}$ varies with time.

As it is well known, there are no precessional motions when the direction of the total angular velocity coincides with the direction of $\mathbf{G}$, it only happens when any of the principal axes of the gyrostat coincides with the fixed direction of $\mathbf{G}$. In this situation, the gyrostat maintains a constant orientation with respect to the space frame $\mathcal{S}$. So, if the gyrostat has initially a precessional motion, it would be interesting to reorientate the gyrostat in such a way that one of its principal axes can be parallel to $\mathbf{G}$. This reorientation or spin-up process can be achieved by means of relative rotational motions of rotors with respect to the platform. These rotors are activated by internal forces.

In this section we analyze the effect of the perturbation in the reorientation process. We consider a free gyrostat with a rotor in relative motion. The axis of this rotor coincides with the principal axis $\mathbf{b}_3$ of the gyrostat. We have modeled the internal forces that move the rotor supposing the relative angular momentum of the rotor h_z is a linear function of time, with a slow variation, that is, $dh_z/dt = \varepsilon \ll 1$. We have chosen the space frame $\mathcal{S}$ in such a way that the $\mathbf{s}_3$-axis coincides with the fixed direction of $\mathbf{G}$, and we want that the final orientation of the gyrostat is that of the principal axis $\mathbf{b}_3$ to be parallel to $\mathbf{G}$. With this choice of the space frame $\mathcal{S}$, the relation between the Euler angles and the components of $\mathbf{G}$ in the body frame $\mathcal{B}$ takes the form

$$\begin{cases} G_x = G\,\sin\psi\,\sin\theta\,, \\ G_y = G\,\cos\psi\,\sin\theta\,, \\ G_z = G\,\cos\theta\,. \end{cases}$$

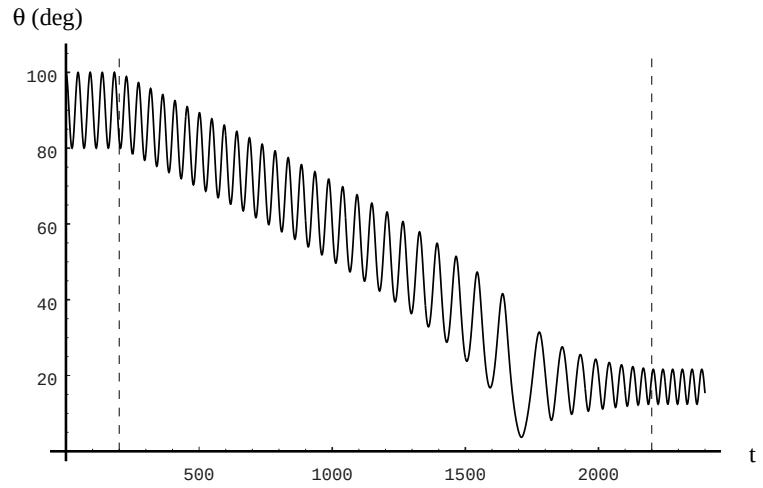

Fig. 8. Time evolution of the nutation angle as h_z increases from 0 to 0.8 and for initial conditions $\theta_0 = 100^\circ$ and $\psi_0 = 90^\circ$. $a_{10} = 0.1$, $a_2 = 0.2$ and $a_3 = 0.3$.

Therefore, when the gyrostat has the orientation we want, $G = G_z$, or what is the same, $\theta = 0$.

Figure 7 shows the evolution of the phase space of the unperturbed gyrostat in the body frame $\mathcal{B}$, as the relative angular momentum h_z of the rotor increases. In this figure, it appears in gray the set of initial conditions for which the rotor spin reorientates the gyrostat ($a_{10} = 0.1$, $a_2 = 0.2$, $a_3 = 0.3$) with a final nutation angle $\theta_f < 20^\circ$. It can be seen in the way this gray area travels from the principal axis $\mathbf{b}_1$ to $\mathbf{b}_3$ as h_z increases from 0 to a final value of 0.8. In this evolution we can also observe that after two different bifurcations, there are no homo/heteroclinic trajectories in the phase space of the unperturbed system.

On the other hand, the time evolution of the nutation angle θ corresponding to one trajectory for which the rotor spin produces the correct reorientation, $\theta_f < 20^\circ$, of the unperturbed gyrostat, is presented in Fig. 8. The initial conditions of this trajectory are $\theta_0 = 100^\circ$ and $\psi_0 = 90^\circ$. The two vertical dashed lines represent the instants when the rotor is turned on and when it reaches the value $h_{z\,\max} = 0.8$ and its acceleration is stopped. This figure reflects how the nutation angle decreases from a mean initial value around 90° to a mean final value around 17°. So, in this way the precessional and nutational motions of the gyrostats can be strongly decreased.

In order to analyze the effect of the perturbation in the reorientation process by rotor spin, we have simulated the maneuver by means of numerical integration of the equations of motion of the perturbed system while the relative angular momentum h_z increases linearly from 0 to a maximum value 0.8. The final goal is to study the influence of the frequency ν and amplitude ε of the perturbation in the change of these areas of suitable initial conditions for a correct reorientation. So, we have made different numerical simulations varying the frequency ν for a fixed amplitude ε and vice versa. For each pair of values (ε, ν) we have created a map with coordinates of initial conditions (ψ_0, θ_0) from 50° to 130° with steps of 1°. At every point of these maps we have indicated the mean final nutation angle θ_f of the perturbed gyrostat after the rotor has reached its maximum relative angular momentum $h_{z\,\max} = 0.8$.

As it can be seen in Fig. 7, the suitable initial conditions for the correct reorientation ($\mathbf{b}_3$ approximately parallel to $\mathbf{G}$) in the unperturbed system are situated in two symmetric approximately circular areas around the axis $\mathbf{b}_1$. On the other hand, Fig. 9 shows six maps corresponding to a perturbed gyrostat for six different increasing values of amplitude ε and a fixed frequency $\nu = 0.1$. In the x–axis is represented the initial nutation angle θ_0 in degrees, and in the y-axis the initial spin angle ψ_0 also in degrees. The continued closed line indicates the border of the area of suitable initial conditions for a correct orientation with $\theta_f < 30^\circ$ when the gyrostat is unperturbed. The gray regions represent the suitable initial conditions for that correct reorientation for the perturbed gyrostat. In this figure, it can be observed how the region of suitable initial conditions is progressively broken up as the

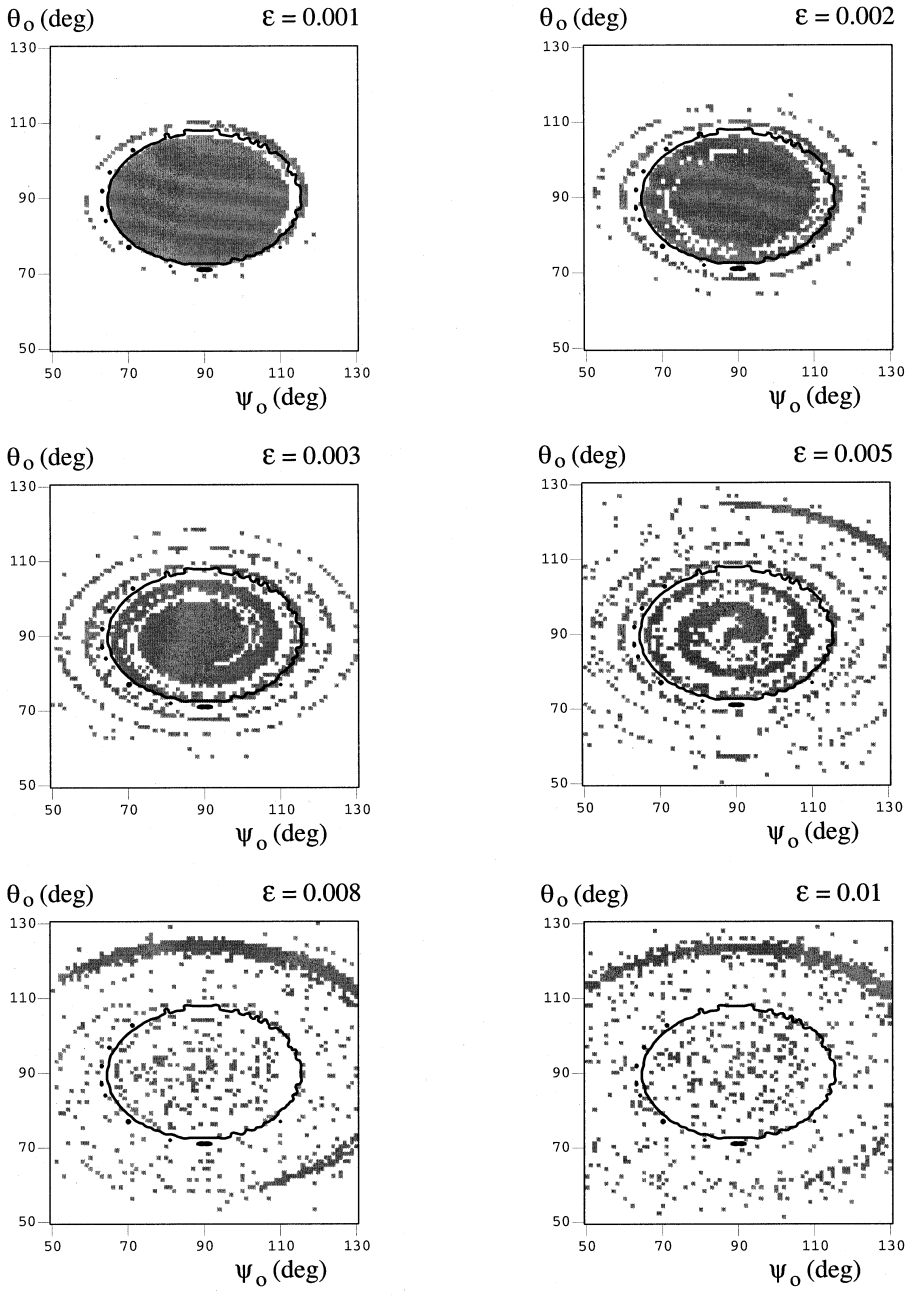

Fig. 9. Evolution of the set of suitable initial conditions for a reorientation with $\theta_f < 30^\circ$, as the amplitude ε increases for fixed frequency $\nu = 0.1$. $a_{10} = 0.1$, $a_2 = 0.2$ and $a_3 = 0.3$.

amplitude ε increases. For $\varepsilon = 0.001$, the area of suitable initial conditions is almost identical to the corresponding one in the unperturbed system. Nevertheless, for $\varepsilon = 0.01$, there is no well-defined area of suitable initial conditions, but they are spread in an almost uniform way over the whole set of initial conditions (ψ_0, θ_0), that is, they are spread in a random way. This means that for relative great values of the amplitude ε the reorientation process of the gyrostat turns to be very chaotic.

Figure 10 presents other six maps of final nutation angle θ_f. These six maps correspond to a fixed amplitude $\varepsilon = 0.01$ and six increasing values of the frequency ν. In this figure it can be seen that for great or small values of frequency, the region of suitable initial conditions for a correct reorientation $(\theta_f < 30^\circ)$ almost coincides with the corresponding area for the unperturbed gyrostat. On the other hand, for intermediate values of frequency, e.g. $\nu = 0.1$, those suitable initial conditions are not

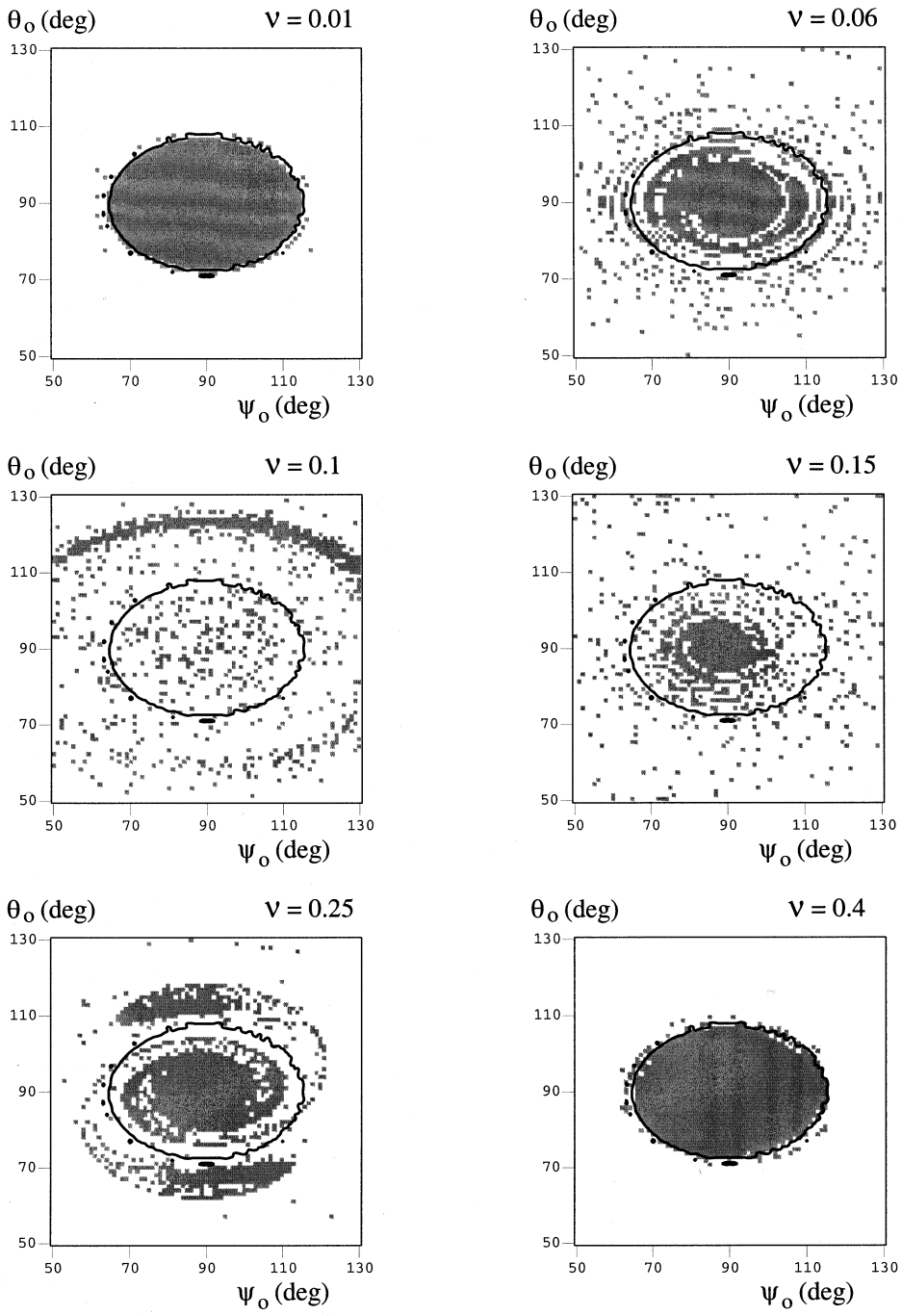

Fig. 10. Evolution of the set of suitable initial conditions for a reorientation with $\theta_f < 30°$, as the frequency ν increases for fixed amplitude $\varepsilon = 0.01$. $a_{10} = 0.1$, $a_2 = 0.2$ and $a_3 = 0.3$.

grouped in a defined area, but they are spread at random over the whole map (ψ_0, θ_0).

Thus, from Figs. 9 and 10 we can conclude that the main effect of the perturbation in the gyrostat reorientation is that, for great amplitudes or intermediate frequencies, the reorientation process turns highly random and chaotic.

5.1. *The measure of the amount of apparent chaotic motion in the reorientation process*

The discussion above leads to the definition of a dimensionless parameter that give us information about the amount of randomness in the reorientation process in terms of the amplitude ε

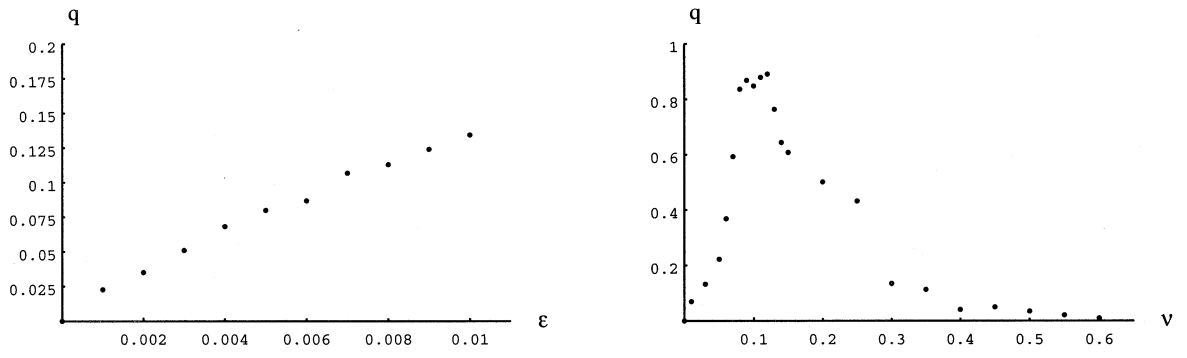

(a) (b)

Fig. 11. The parameter q as a function of (a) the amplitude ε ($\nu = 0.3$) (b) the frequency ν ($\varepsilon = 0.01$). For the two cases $a_{10} = 0.1$, $a_2 = 0.2$ and $a_3 = 0.3$ and $h_{z\ \max} = 0.8$.

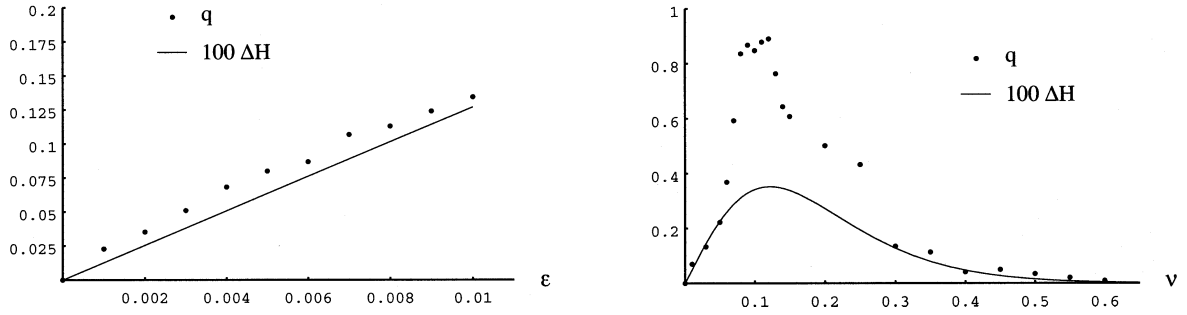

(a) (b)

Fig. 12. The graphs of q and 100 $\Delta\mathcal{H}$. (a) As a function of the amplitude ε for a fixed frequency $\nu = 0.3$. (b) As a function of the frequency ν for a fixed amplitude $\varepsilon = 0.01$. For the two cases $a_{10} = 0.1$, $a_2 = 0.2$, $a_3 = 0.3$ and $h_{z\ \max} = 0.8$.

and the frequency ν. Let us define this parameter, denoted by q, as

$$q = 1 - \frac{\Delta(\nu, \varepsilon)}{\Delta(\nu, 0)}$$

where $\Delta(\nu, 0)$ is the area of initial conditions such that $\theta_f < 30^\circ$ for the unperturbed problem and $\Delta(\nu, \varepsilon)$ is the area of initial conditions with $\theta_f < 30^\circ$ inside $\Delta(\nu, 0)$ for the perturbed problem.

From this definition, we have that as $q \to 1$ the reorientation process turns to be highly random and the area of initial conditions for a desired reorientation with $\theta_f < 30^\circ$ reduces to a collection of points distributed at random in phase space. On the other hand, when $q \to 0$ the reorientation process is well described by the unperturbed problem provided that the areas of ideal initial conditions almost coincide. Roughly speaking, this parameter measures the probability of two close initial conditions to finish close the reorientation process and it can be considered as a measure of the amount of apparent chaotic motion of the reorientation process.

Moreover, Fig. 9 indicates, for a fixed frequency, that the bigger the amplitude ε the greater the parameter q, suggesting a possible linear dependence of ε. On the other hand, when ε is fixed, Fig. 10 indicates that for low frequencies the parameter q is close to zero increasing its value to reach a maximum and to decrease asymptotically to zero, according to the two integrable limits for $\nu = 0$ and $\nu \to \infty$. This behavior is observed for the width of the stochastic layer when the rotors are at rest. In fact, the width of the stochastic layer with the rotors at rest is no more than another indicator of the amount of apparent chaotic motion of the system, and it is not surprising to be connected with the parameter q provided that the wider the stochastic layer is, the more easily the reorientation process will become random.

In order to show the connection between these two measures of the amount of apparent chaotic motion, we proceed to plot the parameter q as a function of the amplitude ε and the frequency ν. Figure 11(a) indicates, for a fixed frequency $\nu = 0.3$,

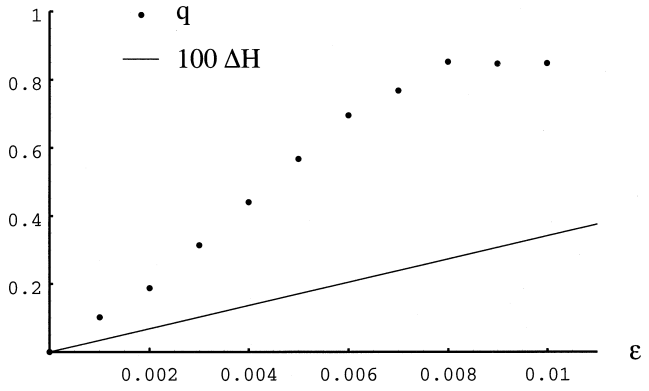

Fig. 13. The parameter q and 100 $\Delta\mathcal{H}$ as a function of the amplitude ε for a fixed frequency $\nu = 0.1$ being $a_{10} = 0.1$, $a_2 = 0.2$, $a_3 = 0.3$ and $h_{z\ \max} = 0.8$.

that q behaves as a linear function, as we expected. On the other hand, Fig. 11(b) shows, for a fixed amplitude $\varepsilon = 0.01$, that the parameter q increases from zero until it reaches a maximum to decrease asymptotically to zero.

The behavior observed in Fig. 11 is the same observed in Fig. 4 corresponding to the graph of the width of the stochastic layer as a function of the amplitude ε and the frequency ν. To emphasize this point we plot in Fig. 12 both the graph of parameter q and 100 $\Delta\mathcal{H}$, a hundred times the width of the stochastic layer.

It is clear that there is a good agreement when both parameters q and 100 $\Delta\mathcal{H}$ are considered as a function of the amplitude ε for the fixed value of the frequency $\nu = 0.3$. On the contrary, when they are plotted as a function of the frequency ν, for a fixed value of $\varepsilon = 0.01$, only good agreement is observed for low and high frequencies, that is, near the two integrable limits and it is in an intermediate range of frequencies where we observe strong deviations. Moreover, these deviations are also observed plotting q as a function of the amplitude ε in the intermediate range of frequencies as it is depicted in Fig. 13 for $\nu = 0.1$.

It is worth to note that the same kind of deviations were observed between the theoretical and numerical estimations of the width of the stochastic layer. These deviations can be explained taking into account the effect of nonlinear resonances. To begin with, we show a graphical description of this phenomenon where we notice the sudden increment of the stochastic layer when a resonant orbit is engulfed. Figure 14(a) shows a 10:1 resonant orbit near the border of the stochastic layer, just before it is absorbed. In Fig. 14(b) we appreciate the absorption of the resonant orbit and the sudden increment of the width of the stochastic layer due to the width of the resonant configuration, the resonant bandwidth. This abrupt increment for the values of Fig. 14 matches with the increment detected numerically and depicted in Fig. 5(b).

As we can see, the abrupt changes in the measure of the amount of apparent chaotic motion of the system are originated for the presence of resonant orbits in the vicinity of the stochastic layer. Our next step is, thus, to establish the existence of

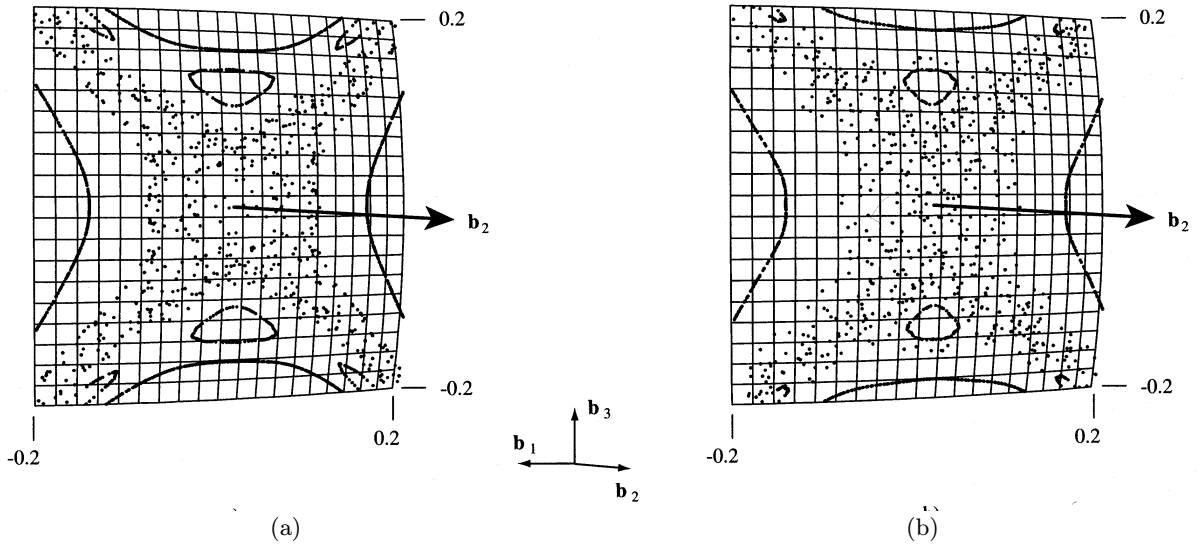

Fig. 14. Absorption of a 10:1 resonant orbit for increasing ε and a fixed frequency $\nu = 0.5$ being $a_{10} = 0.1$, $a_2 = 0.2$ and $a_3 = 0.3$. (a) $\varepsilon = 0.008$. (b) $\varepsilon = 0.014$.

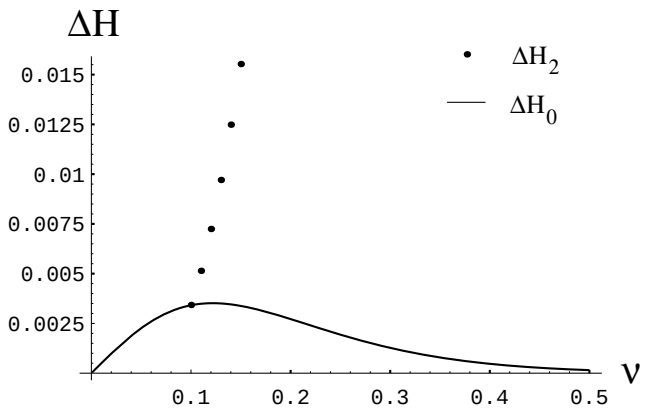

Fig. 15. Overlapping of the primary stochastic layer and the 2:1 resonant band for $\varepsilon = 0.01$, $a_{10} = 0.1$, $a_2 = 0.2$ and $a_3 = 0.3$.

resonant orbits and estimate the width of the resonant band.

6. The Effect of Nonlinear Resonances

Nonlinear resonances are an essential property of nonlinear dynamical systems and it characterizes the response to an external perturbation. The effect of the perturbation is well understood if the perturbation is developed as a double Fourier series [Chirikov, 1979; Zaslavsky *et al.*, 1991]. In fact, if $\omega(I)$ is the frequency of the unperturbed system and ν the frequency of the perturbation, whenever the resonance condition

$$m\omega(I) - n\nu = 0$$

is satisfied, m hyperbolic critical points connected by heteroclinic orbits that encircle m elliptic points will appear in a phase space rotating with frequency $n\nu$. Besides, in the vicinity of the former heteroclinic orbits, resonance stochastic layers may appear as a consequence of the splitting of the separatrices.

This universal phenomenon will allow us to explain the deviations observed between the parameter q and the scaled Melnikov's integral and, at the same time, the deviations between the numerical and theoretical estimations of the width of the stochastic layer. In this way, we will use the Melnikov's subharmonic analysis (for details see, e.g. [Guckenheimer & Holmes, 1983]). Let us consider a system

$$\dot{\mathbf{x}} = f(\mathbf{x}) + \varepsilon g(\mathbf{x}, t) \tag{26}$$

where g is T-periodic in t and for $\varepsilon = 0$ the system is Hamiltonian, possesses a homoclinic orbit $q^0(t)$, to a hyperbolic point p_0 and the interior of $\Gamma^0 = \{q^0(t) \| t \in \mathbb{R}\} \bigcup \{p_0\}$ is filled with a continuous family of periodic orbits $q^\alpha(t)$, $\alpha \in (-1, 0)$. Under these assumptions, we define the subharmonic Melnikov function as

$$M^{m/n}(t_0) = \varepsilon \int_0^{mT_0} \{f(q^\alpha(t)); g(q^\alpha(t), t + t_0)\}\, dt\,, \tag{27}$$

where $q^\alpha(t)$ is a periodic orbit of period $T_\alpha = mT/n$. Then, the following result holds

Theorem 1. *If $M^{m/n}(t_0)$ has simple zeroes and is independent of ε, then for ε sufficiently small (26) has a subharmonic orbit of period mT. Besides, if $M^{m/1}(t_0) = M^m(t_0)$, then*

$$\lim_{m \longrightarrow \infty} M^m(t_0) = M(t_0)\,,$$

where $M(t_0)$ is the Melnikov function of (26).

6.1. *Subharmonic analysis*

The previous result is the tool we need to prove the existence of subharmonic resonant orbits for a perturbed gyrostat with no spinning rotors, that is, for the system

$$\mathcal{H} = \frac{1}{2}(a_1 g_1^2 + a_2 g_2^2 + a_3 g_3^2) + \frac{1}{2}\varepsilon g_1^2 \cos(\nu t)\,. \tag{28}$$

First of all, we have to derive the expression of the frequency of the gyrostat when it behaves as a rigid body, that is, for the unperturbed system ($\varepsilon = 0$). From Eqs. (17) and (18) we observe that G_x, G_y and G_z are periodic functions with period

$$\begin{cases} T = \dfrac{n_1}{F(\pi/2,\, k_1)}, & \mathcal{H} < \dfrac{a_2}{2} \\ T = \dfrac{n_3}{F(\pi/2,\, 1/k_1)}, & \mathcal{H} > \dfrac{a_2}{2} \end{cases}$$

So, we define a frequency $\omega = 2\pi/T$, which results in the frequency of the angular variable when the Hamiltonian is expressed in action angle variables. Indeed, let us introduce a pair of conjugate canonical variables (L, ℓ), similar to Serret–Andoyer [Deprit, 1967; Deprit & Elipe, 1993], which are cylindrical coordinates of vector $\mathbf{G}$

$$G_x = \sqrt{1 - L^2}\cos\ell, \quad G_y = L\,,$$
$$G_z = \sqrt{1 - L^2}\sin\ell\,.$$

By inversion, L and ℓ are periodic functions with the same period as G_x, G_y and G_z. Thus, the action is given by

$$I = \frac{1}{2\pi}\int_0^T L(t)\dot{\ell}(t)\,dt$$

and then,

$$\omega = \frac{\partial \mathcal{H}}{\partial I} = \frac{1}{\partial I/\partial \mathcal{H}}$$

where

$$\frac{\partial I}{\partial \mathcal{H}} = \frac{1}{2\pi}\left[\frac{\partial T}{\partial \mathcal{H}}L(T)\dot{\ell}(t) + \int_0^T \frac{\partial L}{\partial \mathcal{H}}\dot{\ell}\,dt + \int_0^T L\frac{\partial \dot{\ell}}{\partial \mathcal{H}}\,dt\right].$$

Taking into account the initial condition $L(0) = 0$ we obtain

$$\omega = \frac{2\pi}{T}.$$

Therefore, we have a $m:n$ nonlinear resonance when

$$\begin{aligned} \frac{mT_0}{n} &= \frac{4K(k_1)}{n_1}, \quad \mathcal{H}_0 < \frac{a_2}{2} \\ \frac{mT_0}{n} &= \frac{4K(1/k_1)}{n_3}, \quad \mathcal{H}_0 > \frac{a_2}{2} \end{aligned} \tag{29}$$

where $T_0 = 2\pi/\nu$.

From the above resonance condition (29) and for $\varepsilon \neq 0$ we can establish the following theorem.

Theorem 2. *The system (28) has resonant subharmonic orbits of period mT_0/n, for even m and $n = 1$.*

Proof. The proof is quite straightforward by computing the subharmonic Melnikov function and applying Theorem 1.

For the case $\mathcal{H}_0 < a_2/2$, we obtain

$$M^{m/n}(t_0) = \int_0^{mT_0} (a_2 - a_3)\varepsilon\Gamma_1\Gamma_2\Gamma_3 \mathrm{sn}(n_1 t,\, k_1)\mathrm{cn}(n_1 t,\, k_1)\mathrm{dn}(n_1 t,\, k_1)\cos\nu(t + t_0)\,dt\,.$$

Basic considerations about the parity of the functions involved in the integral yields after expanding $\cos\nu(t + t_0)$ to

$$M^{m/n}(t_0) = (a_3 - a_2)\varepsilon\Gamma_1\Gamma_2\Gamma_3 \int_0^{mT_0} \mathrm{sn}(n_1 t,\, k_1)\mathrm{cn}(n_1 t,\, k_1)\mathrm{dn}(n_1 t,\, k_1)\sin\nu t\sin\nu t_0\,dt\,.$$

Introducing a new variable $z = n_1 t$ and integrating by parts

$$u = \sin\frac{m\pi z}{2nK}, \quad dv = \mathrm{sn}(z,\, k_1)\mathrm{cn}(z,\, k_1)\mathrm{dn}(z,\, k_1)dz$$

we obtain

$$M^{m/n}(t_0) = \frac{(a_3 - a_2)m\pi\varepsilon\Gamma_1\Gamma_2\Gamma_3}{4nn_1K}\sin\nu t_0 \int_0^{4nK} \mathrm{sn}^2(z,\, k_1)\cos\frac{m\pi z}{2nK}\,dz\,.$$

From the Fourier series of the function $\mathrm{sn}^2(z,\, k_1)$ [Abad *et al.*, 1994; Vallejo, 1995]

$$\mathrm{sn}^2(z,\, k_1) = \frac{E - K}{k_1^2 K} - \frac{2\pi^2}{k_1^2 K^2}\sum_{m=1}^{\infty}\frac{mq^m}{1 - q^{2m}}\cos\frac{m\pi z}{K}\,,$$

the subharmonic integral vanishes unless $n = 1$ and even m, that is to say, for $m = 2\overline{m}$, $\overline{m} \in \mathbb{N}$. Thus, we obtain

$$M^m(t_0) = \frac{(a_2 - a_3)m\pi\varepsilon\Gamma_1\Gamma_2\Gamma_3}{2n_1K}\sin\nu t_0 \frac{2\pi^2}{k_1^2 K}\frac{\overline{m}q^{\overline{m}}}{1 - q^{2\overline{m}}}$$

where $q = e^{-\pi K'/K}$ and then

$$M^m(t_0) = \frac{(a_2 - a_3)\overline{m}^2\pi^3\varepsilon\Gamma_1\Gamma_2\Gamma_3}{n_1 k_1^2 K^2 \sinh\dfrac{\overline{m}\pi K'}{K}}\sin\nu t_0\,.$$

Finally, from the resonance condition (29), we have

$$M^m(t_0) = \frac{(a_2 - a_3)\pi\varepsilon\nu^2\Gamma_1\Gamma_2\Gamma_3}{n_1^3 k_1^2 \sinh\dfrac{K'\nu}{n_1}}\sin\nu t_0$$

which possesses simple zeroes and it is independent of ε for even m. Thus, by Theorem 1, the system

(28) has subharmonic orbits with period mT_0 for even m.

Besides, taking into account that

$$\lim_{m\longrightarrow\infty} 2\mathcal{H} = a_2\,, \quad \lim_{m\longrightarrow\infty} K' = \frac{\pi}{2}\,,$$

$$\lim_{m\longrightarrow\infty} k_1 = 1$$

we obtain that

$$\lim_{m\longrightarrow\infty} M^m(t_0) = 2M(t_0) = \frac{(a_3-a_2)\pi\varepsilon\nu^2}{(a_3-a_1)n_2^2\sinh\dfrac{\pi\nu}{2n_2}}\,.$$

Note that this result is the same in Theorem 1 but is a factor 2. This is because the Melnikov subharmonic integral has been calculated for one of the heteroclinic orbits, but a periodic orbit has a pair of heteroclinic orbits as limit. ■

A similar conclusion is obtained for $\mathcal{H}_0 > a_2/2$. In this case the subharmonic Melnikov integral is

$$M^m(t_0) = \frac{(a_2-a_3)k_1^2\pi\nu^2\varepsilon\Gamma_1\gamma_2\Gamma_3}{n_3^3\sinh\dfrac{K'\nu}{n_3}}\sin\nu t_0\,.$$

6.2. *The resonant bandwidth*

Once established the existence of resonant orbits, we focus on the theoretical estimation of the resonant bandwidth with the aim to see how the primary stochastic layer shows an abrupt increment when a resonant orbit is engulfed.

There exists a theoretical estimation for the resonant bandwidth for two degrees of freedom systems of the form [Perko, 1992]

$$\mathcal{H}_\varepsilon(p,\,q,\,\theta,\,I) = F(p,\,q) + G(I) + \varepsilon\mathcal{H}_1(q,\,p,\,\theta,\,I)$$

where $\mathcal{H}_0 = F(p,\,q) + G(I)$ is an integrable Hamiltonian, $G'(I) > 0$ for $I > 0$ and the $(p,\,q)$ phase plane contains hyperbolic saddles connected by homoclinic or heteroclinic orbits filled with periodic orbits. Although the system (28) does not match this structure, it is possible to reduce it by means of a canonical extension of the variables. Thus, we obtain the following formula for the estimation of the resonant bandwidth

$$\Delta\mathcal{H}_m = 2\omega(\mathcal{H}_m)\sqrt{\frac{M^m_{\max}-M^m_{\min}}{\pi\overline{\omega}^m}}$$

where

$$\overline{\omega}^m = -T_0\omega(\mathcal{H}_m)\frac{d\omega(\mathcal{H}_m)}{d\mathcal{H}}$$

being $\mathcal{H}_m$ the energy corresponding to the resonant orbit, that is to say $\omega(\mathcal{H}_m) = \nu/m$. Taking into account that

$$\frac{d\omega(\mathcal{H}_m)}{d\mathcal{H}} = \frac{n_1[(a_2-2\mathcal{H})K(k_1) - (a_2-a_1)E(k_1)]}{4(2\mathcal{H}-a_1)(a_2-2\mathcal{H})K^2(k_1)}$$

we yield, finally, to

$$\Delta\mathcal{H}_m = \sqrt{\frac{16(2\mathcal{H}-a_1)(a_2-2\mathcal{H})(a_2-a_3)K^2(k_1)\nu^4\varepsilon\Gamma_1\Gamma_2\Gamma_3}{n_1^4\pi m k_1^2[(a_2-2\mathcal{H})K(k_1) - (a_2-a_1)E(k_1)]\sinh\dfrac{K'\nu}{n_1}}}\,, \tag{30}$$

where Γ_1, Γ_2 and Γ_3 are the coefficients appearing in Eqs. (17).

The formula (30) will help us to show how the stochastic layer and the resonant bands overlap. Then, we can account this effect to improve the estimation of the width of the stochastic layer and, in the last resort, to establish a better agreement between the two measures of the amount of apparent chaotic motion of the system.

We take, as an example, the 2:1 resonance. In this case we can calculate the values of the frequency ν for which the stochastic layer and the resonant band overlap. Figure 15 shows the overlap for a gyrostat with $a_{10} = 0.1$, $a_2 = 0.2$, $a_3 = 0.3$ and $\varepsilon = 0.01$. We can appreciate that the overlapping begins for $\nu \approx 0.1$ (for smaller values the resonant band is entirely inside the stochastic layer) and it finishes for $\nu \approx 0.15$ (for greater values the resonant band is outside the stochastic layer disappearing for ν great enough). Note that the forming pick in Fig. 15 explains the abrupt increment for both the numerical estimation of the width of the stochastic layer and the parameter q in the range of frequencies between 0.1 and 0.15 [compare Fig. 15 with Figs. 6 and 11(b)].

7. Conclusions

We have established that for the model of a gyrostat with time-dependent moments of inertia chaotic

behavior takes place when the rotors are at relative rest. Moreover, analytical and numerical estimations of the width of the stochastic layer have been obtained, showing the discrepancies between both of them. This chaotic behavior is responsible for the randomness observed in the reorientation process which is measured by means of a suitable parameter. Finally, we take into account the effect of the nonlinear resonances to explain the sudden increment of the amount of apparent chaotic motion of the system and the discrepancies observed between the numerical and theoretical estimations of the width of the stochastic layer.

Acknowledgments

This work has been partially supported by Universidad de La Rioja (ATUR97/029, ATUR98/11 and API-98/A11).

References

Abad, A., Elipe, A. & Vallejo, M. [1994] "Automated fourier series expansions for elliptic functions," *Mech. Res. Commun.* **21**, 361–366.

Cavas, J. A. & Vigueras, A. [1994] "An integrable case of a rotational motion analogous to that of Lagrange and Poisson for a gyrostat in a Newtonian force field," *Celest. Mech. Dyn. Astro.* **60**, 317–330.

Chirikov, B. V. [1979] "A universal instability of many-dimensional oscillator systems," *Phys. Rep.* **52**, 263–379.

Cochran, J. E., Shu, B. H. & Rews, S. D. [1982] "Attitude motion of asymmetric dual-spin spacecraft," *J. Guidance Contr. Dyn.* **5**, 37–42.

Cochran, J. E. & Shu, P. H. [1983] "Attitude motion of spacecraft with skewed internal angular momenta," *The J. Astronaut. Sci.* **XXXI**, 203–215.

David, D., Holm, D. & Tratnik, M. V. [1990] "Hamiltonian chaos in nonlinear optical polarization dynamics," *Phys. Rep.* **187**, 281–367.

Deprit, A. [1967] "Free rotation of a rigid body studied in phase plane," *Am. J. Phys.* **35**, 424–428.

Deprit, A. & Elipe, A. [1993] "Complete reduction of the Euler–Poinsot problem," *J. Astronaut. Sci.* **41**, 603–628.

Elipe, A. & Ferrer, S. [1994] "Reductions, relative equilibria and bifurcations in the generalized van der Waals potential: Relation to the integrable cases," *Phys. Rev. Lett.* **72**, 985–988.

Elipe, A., Arribas, M. & Riaguas, A. [1997] "Complete analysis of bifurcations in the axial gyrostat problem," *J. Phys.* **A30**, 587–601.

Elipe, A. & Lanchares, V. [1997a] "Phase flow of an axially symmetrical gyrostat with one constant rotor," *J. Math. Phys.* **38**, 3533–3544.

Elipe, A. & Lanchares, V. [1997b] "Two equivalent problems: Gyrostats in free motion and parametric quadratic Hamiltonians," *Mech. Res. Commun.* **24**, 583–590.

Frauendiener, J. [1995] "Quadratic Hamiltonians on the unit sphere," *Mech. Res. Commun.* **22**, 313–317.

Goldstein, H. [1992] *Mecánica Clásica* (Editorial Reverté, Barcelona).

Gradshteyn, I. S. & Ryzhik, I. M. [1980] *Table of Integrals, Series and Products* (Academic Press, San Diego).

Guckenheimer, J. & Holmes, P. [1983] *Nonlinear Oscillations, Dynamical Systems and Bifurcations of Vector Fields* (Springer-Verlag, NY).

Hall, C. D. & Rand, R. H. [1994] "Spinup dynamics of axial dual spin spacecraft," *J. Guidance Contr. Dyn.* **17**, 30–37.

Hall, C. D. [1995a] "Spinup dynamics of gyrostats," *J. Guidance Contr. Dyn.* **18**, 1177–1183.

Hall, C. D. [1995b] "Resonance capture in axial gyrostats," *The J. Astronaut. Sci.* **43**, 127–138.

Hall, C. D. [1995c] "Spinup dynamics of biaxial gyrostats," *The J. Astronaut. Sci.* **43**, 263–275.

Hall, C. D. [1996] "Momentum transfer in two–rotor gyrostats," *J. Guidance Contr. Dyn.* **19**, 1157–1161.

Hall, C. D. [1997] "Momentum transfer dynamics of a gyrostat with a discrete damper," *J. Guidance Contr. Dyn.* **20**, 1072–1075.

Holmes, P. J. & Marsden, J. E. [1983] "Horseshoes and Arnold diffusion for Hamiltonian systems on Lie groups," *Indiana Univ. Math. J.* **32**, 273–309.

Hubert, C. H. [1980] *An Attitude Acquisition Technique for Dual–Spin Spacecraft*, Ph.D. Cornell University, Ithaca, NY.

Hughes, P. C. [1986] *Spacecraft Attitude Dynamics*, (John Wiley, NY).

Iñarrea, M. [1998] *Método de Melnikov, bandas de estocasticidad y no integrabilidad en un giróstato con momentos de inercia variables*, Ph.D. Publicaciones del Seminario Matemático García Galdeano. Serie II, **64**, Universidad de Zaragoza.

Koiller, J. [1984] "A mechanical system with a 'wild' horseshoe," *J. Math. Phys.* **25**, 1599–1604.

Kramers, H. A. [1923] "Über die quantelung rotierender moleküle," *Z. Phys.* **13**, 343–350.

Krishnaprasad, P. S. [1985] "Lie–Poisson structures, dual-spin spacecraft and asymptotic stability," *Nonlin. Anal. Th. Meth. Appl.* **9**, 1011–1035.

Lambert, J. D. [1976] *Computational Methods in Ordinary Differential Equations* (John Wiley, London).

Lanchares, V. & Elipe, A. [1995a] "Bifurcations in biparametric quadratic potentials," *Chaos* **5**, 367–373.

Lanchares, V. & Elipe, A. [1995b] "Bifurcations in biparametric quadratic potentials II," *Chaos* **5**, 531–535.

Lanchares, V., Iñarrea, M. Salas, J. P., Sierra, J. D. & Elipe, A. [1995] "Surfaces of bifurcation in a triparametric quadratic Hamiltonian," *Phys. Rev.* **E52**, 5540–5548.

Lanchares, V., Iñarrea, M. & Salas, J. P. [1998] "Spin rotor stabilization of a dual–spin spacecraft with time dependent moments of inertia," *Int. J. Bifurcation and Chaos* **8**, 609–617.

Peano, G. [1895a] "Sopra lo spostamento del polo sulla terra," *Atti. R. Accad. Sci. Torino* **30**, 515–523.

Peano, G. [1895b] "Sul moto del polo terrestre," *Atti. R. Accad. Sci. Torino* **30**, 845–852.

Perko, L. M. [1992] "Melnikov's method, stochastic layers and nonintegrability of a perturbed Duffing–oscillator," *Rocky Mountain J. Math.* **22**, 973–1000.

Ring, P. & Schuck, P. [1980] *The Nuclear Many-Body Problem* (Springer-Verlag, NY).

Thomson, W. T. [1986] *Introduction to Space Dynamics* (Dover Publications, NY).

Tong, X., Tabarrok, B. & Rimrott, F. P. J. [1995] "Chaotic motion of an asymmetric gyrostat in the gravitation field," *Int. J. Non-Lin. Mech.* **30**, 191–203.

Vallejo, M. [1995] *Serie de Fourier de funciones elípticas. Aplicación a la Precesión Terrestre*, Ph.D. Boletín ROA, No. 2/95, Real Instituto y Observatorio de la Armada en San Fernando, Cádiz.

Volterra, V. [1899] "Sur la théorie des variations des latitudes," *Acta Math.* **22**, 201–358.

Wiesel, W. E. [1997] *Spaceflight Dynamics*, 2nd edition (McGraw–Hill, NY).

Zaslavsky, G. M., Sagdeev, R. Z., Usikov, D. A. & Chernikov, A. A. [1991] *Weak Chaos and Quasi-Regular Patterns* (Cambridge University Press, Cambridge).